

RESEARCH ARTICLE

10.1002/2016JF004183

Slow-slip events on the Whillans Ice Plain, Antarctica, described using rate-and-state friction as an ice stream sliding law

Bradley Paul Lipovsky^{1,2}  and Eric M. Dunham^{1,3} 

¹Department of Geophysics, Stanford University, Stanford, California, USA, ²Department of Earth and Planetary Sciences, Harvard University, Cambridge, Massachusetts, USA, ³Institute for Computational and Mathematical Engineering, Stanford University, Stanford, California, USA

Key Points:

- We validate a laboratory-derived sliding law, rate-and-state friction, as an ice stream basal sliding law
- Stick-slip cycles on the Whillans Ice Plain, West Antarctica, occur in the slow-slip limit of sliding behavior
- Rate-and-state friction captures the transition between tidally modulated stick-slip motion and quasi-steady tidal modulation

Supporting Information:

- Figure S1
- Figure S2
- Figure S3
- Supporting Information S1

Correspondence to:

B. P. Lipovsky,
brad_lipovsky@fas.harvard.edu

Citation:

Lipovsky, B. P., and E. M. Dunham (2017), Slow-slip events on the Whillans Ice Plain, Antarctica, described using rate-and-state friction as an ice stream sliding law, *J. Geophys. Res. Earth Surf.*, 122, doi:10.1002/2016JF004183.

Received 20 DEC 2016

Accepted 29 MAR 2017

Accepted article online 5 APR 2017

Abstract The Whillans Ice Plain (WIP), Antarctica, experiences twice daily tidally modulated stick-slip cycles. Slip events last about 30 min, have sliding velocities as high as ~0.5 mm/s (15 km/yr), and have total slip ~0.5 m. Slip events tend to occur during falling ocean tide: just after high tide and just before low tide. To reproduce these characteristics, we use rate-and-state friction, which is commonly used to simulate tectonic faulting, as an ice stream sliding law. This framework describes the evolving strength of the ice-bed interface throughout stick-slip cycles. We present simulations that resolve the cross-stream dimension using a depth-integrated treatment of an elastic ice layer loaded by tides and steady ice inflow. Steady sliding with rate-weakening friction is conditionally stable with steady sliding occurring for sufficiently narrow ice streams relative to a nucleation length. Stick-slip cycles occur when the ice stream is wider than the nucleation length or, equivalently, when effective pressures exceed a critical value. Ice streams barely wider than the nucleation length experience slow-slip events, and our simulations suggest that the WIP is in this slow-slip regime. Slip events on the WIP show a sense of propagation, and we reproduce this behavior by introducing a rate-strengthening region in the center of the otherwise rate-weakening ice stream. If pore pressures are raised above a critical value, our simulations predict that the WIP would exhibit quasi-steady tidally modulated sliding as observed on other ice streams. This study validates rate-and-state friction as a sliding law to describe ice stream sliding styles.

Plain Language Summary The Whillans Ice Plain, a 120 km wide region of the West Antarctic Ice Sheet, experiences slip events that bear similarity to tectonic earthquakes. During a slip event, the entire 120 km region slides forward by about half a meter over a period of about 30 min. Remarkably, on most days these slip events occur just after high tide and just before low tide. These slip events are much slower and have much lower ground accelerations than typical tectonic earthquakes of this size. We create computer simulations of these slip events using a type of friction law originally discovered in the study of tectonic earthquake. We show that the slow-slip events on the Whillans Ice Plain are similar to slow-slip events in subduction zones in that they nucleate over very long distances. Our model also recreates the general type of behavior observed in other parts of Antarctica where slip events do not occur. By better describing the friction at the base of the ice sheet, we hope to improve the computer simulations of ice sheet dynamics that constrain estimates of future sea level rise.

1. Introduction

The complete deceleration, or stagnation, of a single Antarctic ice stream would reduce the Antarctic Ice Sheet's contribution to global mean sea level by ~50% [Rignot *et al.*, 2008; Shepherd *et al.*, 2012; Schoen *et al.*, 2015; Harig and Simons, 2015]. As the only ice stream currently undergoing stagnation, the Whillans Ice Plain (WIP, location map in Figure 1), offers a unique opportunity to quantify the physics of stagnation and thereby reduce uncertainty in future sea level rise estimates [Whillans *et al.*, 2001; Joughin *et al.*, 2002; Stearns *et al.*, 2005; Beem *et al.*, 2014]. Such an effort is complicated, however, by observations that show that WIP ice velocities exhibit twice daily, tidally modulated stick-slip cycles that are reminiscent of the tectonic earthquake cycle [Bindschadler *et al.*, 2003; Wiens *et al.*, 2008]. Despite the need to understand the relationship between stagnation, stick-slip, and ice flux, previous descriptions of ice stream motion [MacAyeal, 1993; Robel *et al.*, 2013; Kyrke-Smith *et al.*, 2014; Bougamont *et al.*, 2011, 2015; Feldmann and Levermann, 2016] have generally been

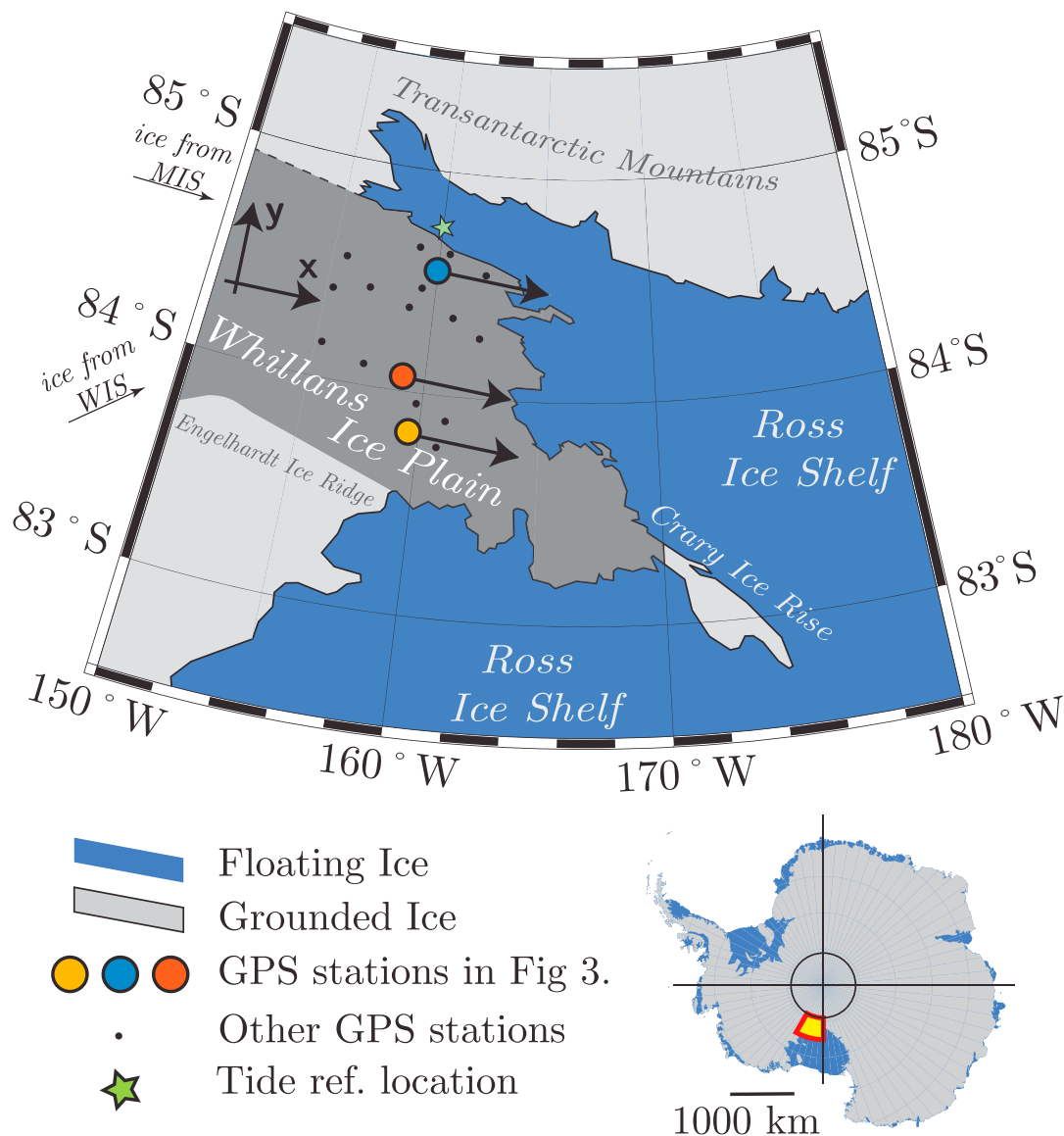


Figure 1. Location and geography of the Whillans Ice Plain (WIP), West Antarctica. Circles show the three GPS stations used in this study; data from the northernmost (yellow) station are plotted in Figure 2, and data from all three stations are plotted in Figure 3. Tide heights in Figure 2 are from the tide model of Padman *et al.* [2002] measured at the location marked with a green star. This figure also shows the (x, y) coordinate system used in this work.

formulated with an eye toward kiloyear-scale dynamics [Heinrich, 1988; Hemming, 2004] and therefore have not incorporated the ice stream basal processes that give rise to stick-slip cycles.

In this work, we introduce an ice stream basal sliding law, rate-and-state friction, that gives rise to either steady sliding or stick-slip cycles, depending on system geometry (e.g., ice stream width) and basal conditions (e.g., effective pressure). Rate-and-state friction is widely used in describing tectonic earthquake behavior and provides a well-posed mathematical framework that captures the evolution of frictional strength and its dependence on both instantaneous sliding velocity and the history of sliding [Dieterich, 1979; Ruina, 1983; Rice and Ruina, 1983; Marone, 1998; Dieterich, 2007; Rice *et al.*, 2001]. As described in more detail in section 3.1, rate-and-state friction consists of both an instantaneous and a time-dependent deviation from a reference frictional strength. This framework has been shown to encompass a wide range of different physical processes across a diversity of systems, both natural and experimental. With respect to glaciology, these include experimental studies of ice sliding against ice [Schulson and Fortt, 2012], ice sliding against rock

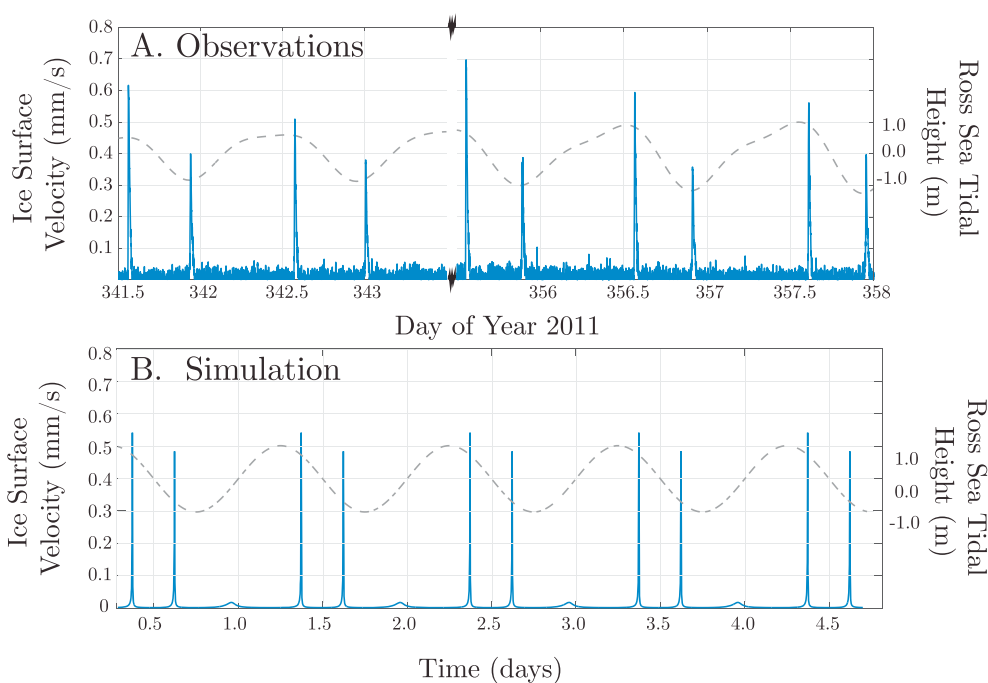


Figure 2. Ice surface velocities (solid blue lines) during 10 tidally modulated stick-slip cycles in (a) data and (b) a simulation. The GPS data are from the station shown in Figure 1 with a yellow circle, and the simulation shown in Figure 2b is described in section 6 and Figure 8a. Also shown is tide height (dashed grey line). In Figure 2a, the tide height is inferred for the location marked in Figure 1, green star. The simulation in Figure 2b includes forcing from a simplified tide with a single, diurnal constituent.

[Zoet *et al.*, 2013; McCarthy *et al.*, 2016, 2017], sliding within a layer of glacial till [Thomson and Iverson, 2008; Rathbun *et al.*, 2008; Rathbun and Marone, 2010; Iverson, 2010], and ice sliding against a rigid-stepped [Zoet and Iverson, 2016] and a rigid sinusoidal [Zoet and Iverson, 2015] bed. We discuss the physical processes that give rise to rate-and-state friction in greater detail in section 3.1.1.

The WIP stick-slip cycles are unique; no other Antarctic ice stream is known to experience stick-slip cycles at such large scale. However, tidally modulated seismicity (with much smaller event sizes) is commonly observed [Anandakrishnan and Bentley, 1993; Anandakrishnan and Alley, 1994; Danesi *et al.*, 2007; Adalgeirsdóttir *et al.*, 2008; Zoet *et al.*, 2012; Smith *et al.*, 2015]. Also commonly observed is tidal modulation of ice stream flow velocity without stick-slip [Anandakrishnan *et al.*, 2003; Gudmundsson, 2006; Marsh *et al.*, 2013; Minchew *et al.*, 2016]. We refer to this latter type of tidally modulated flow as quasi-steady tidal modulation to distinguish it from the case of constant velocity which we simply refer to as steady. As we demonstrate, rate-and-state friction, when coupled to the elastic response of an ice stream and some loading process (either steady or time varying, as in the case of tides), can reproduce this diversity of sliding styles.

The ability to describe both steady sliding and stick-slip cycles distinguishes rate-and-state friction from sliding laws used in previous studies of WIP stick-slip cycles. Bindschadler *et al.* [2003] proposed a simplified stick-slip model where slip events occur when accumulated strain reaches a prescribed failure threshold. This model was refined to include the effects of viscosity [Winberry *et al.*, 2009; Goldberg *et al.*, 2014] and expanded to higher spatial dimensions [Sergienko *et al.*, 2009; Walker *et al.*, 2016]. However, weakening and unstable slip, in these studies, was an imposed consequence of reaching the failure threshold. The one exception to the use of threshold models is Goldberg *et al.* [2014], who analyze ice stream motion under rate-and-state friction (in their supporting information), as well as other more phenomenological sliding laws. The main feature that sets our study apart from the work of Goldberg *et al.* [2014] is our analysis of the transition from steady sliding to stick-slip cycles (i.e., consideration of the conditional nature of sliding instability).

To complete this introduction, we briefly explain several features of rate-and-state friction as they relate to ice stream dynamics. Consider an ice stream loaded by a constant inflow velocity, neglecting, for now, periodic tidal forcing. A necessary, but not sufficient, condition for stick-slip cycles is a rate-weakening steady state

frictional response, that is, a reduction in frictional strength with increasing sliding velocity after sufficient sliding has eliminated memory of the sliding history. As described in detail in section 4, with rate-weakening friction, the occurrence of stick-slip versus steady sliding depends on the elastic compliance of the ice stream. The resulting instability condition (equation (18)) introduces a critical ice stream width or nucleation length, below which the increased elastic stiffness prevents stick-slip response and instead favors steady sliding and above which stick-slip cycles occur even for steady loading. A rigorous derivation of this instability condition is presented in Appendix B1. This nucleation length is inversely proportional to the square root of effective pressure and consequently can become quite large when pore pressure is elevated to a value close to the overburden pressure—exactly the condition expected beneath ice streams [Kamb, 2001; Tulaczyk *et al.*, 2014].

Most tectonic earthquakes occur on fault segments that are much longer than the nucleation length and hence take the form of rapidly propagating ruptures whose advance across the fault is limited by inertia to a rupture velocity close to the speed of elastic waves. We refer to this slip style as fast slip. In contrast, when the fault dimension is comparable to the nucleation length, slip events occur in a more gradual manner known as slow slip, the same style that occurs in subduction zone slow-slip events [Dragert *et al.*, 2001; Rogers and Dragert, 2003; Obara, 2002; Ito *et al.*, 2007; Liu and Rice, 2005, 2007; Peng and Gombert, 2010].

We argue that the WIP slip events are slow-slip events as a consequence of a particular, intermediate range of subglacial effective pressures. Within this range, effective pressures are high enough for stick-slip cycles to occur and yet are low enough to prevent the acceleration to rapid, inertially limited ruptures. One implication of this interpretation is that ice streams may experience a transition from steady sliding to stick-slip cycles if they experience a reduction of pore pressure, provided the bed has rate-weakening frictional properties. From this perspective, stick-slip cycles at WIP are consistent with declining pore pressure being the causative mechanism leading to the stagnation of the WIP [Retzlaff and Bentley, 1993; Alley *et al.*, 1994; Anandakrishnan and Alley, 1997], even if WIP sliding in the past was steady.

In the presence of tidal forcing, an ice stream with rate-weakening friction at its bed responds in a somewhat more complex manner than when loading is only due to a steady inflow of ice from the upstream direction. The general conditions for stick-slip cycles still apply, but the periodic tidal forcing can either introduce a periodic modulation of otherwise steady sliding or alter the timing and size of slip events if the condition for stick-slip cycles is met. For example, our preferred model of the WIP events has parameters that would produce about four slip events per day in the absence of tidal forcing but with tidal forcing features only two events per day that occur just after high tide and just before low tide. This tidal modulation further constrains basal properties beyond the constraints provided by the requirement that events occur in the slow-slip part of parameter space.

In this work, we conduct numerical simulations of ice stream sliding with rate-and-state friction. This study builds on previous models of WIP stick-slip cycles [Winberry *et al.*, 2009; Sergienko *et al.*, 2009; Goldberg *et al.*, 2014; Walker *et al.*, 2016] but explores the diversity of sliding styles that emerge with rate-and-state friction under various conditions. In the following, we first review observational constraints on the WIP events and then introduce the governing equations describing the elastic response of an ice stream with rate-and-state friction at its bed. We then turn to numerical simulations to examine stick-slip cycles and to identify key parameters controlling sliding style, focusing in particular on conditions for slow slip. This is done first without tidal forcing and subsequently with periodic tidal forcing. We successfully reproduce the observed tidal modulation of WIP events. These initial explorations are done for an ice stream with spatially uniform friction and effective pressure at its bed. While such simple models reproduce many aspects of the WIP events, we find it necessary to add spatial heterogeneity to basal friction in order to more closely match several details of the WIP rupture process, in particular the slow rupture velocity. Therefore, we finish our study by adding a minimal degree of heterogeneity in order to bring our model into closer accord with the observations, providing further validation of the relevance of rate-and-state friction to ice stream sliding. We close with a discussion of the implications of rate-and-state friction for more general questions surrounding the response of Antarctic ice streams to changes in pore pressure. The unique sliding style of the WIP provides a window into the dynamics of ice stream sliding and the strength of the ice-bed interface.

2. Observations and Data

The WIP is the downstream extent of both the Whillans Ice Stream (WIS) and part of the Mercer Ice Stream (MIS) as shown in Figure 1. The width of the WIP ranges from about 150 km near the confluence of the MIS

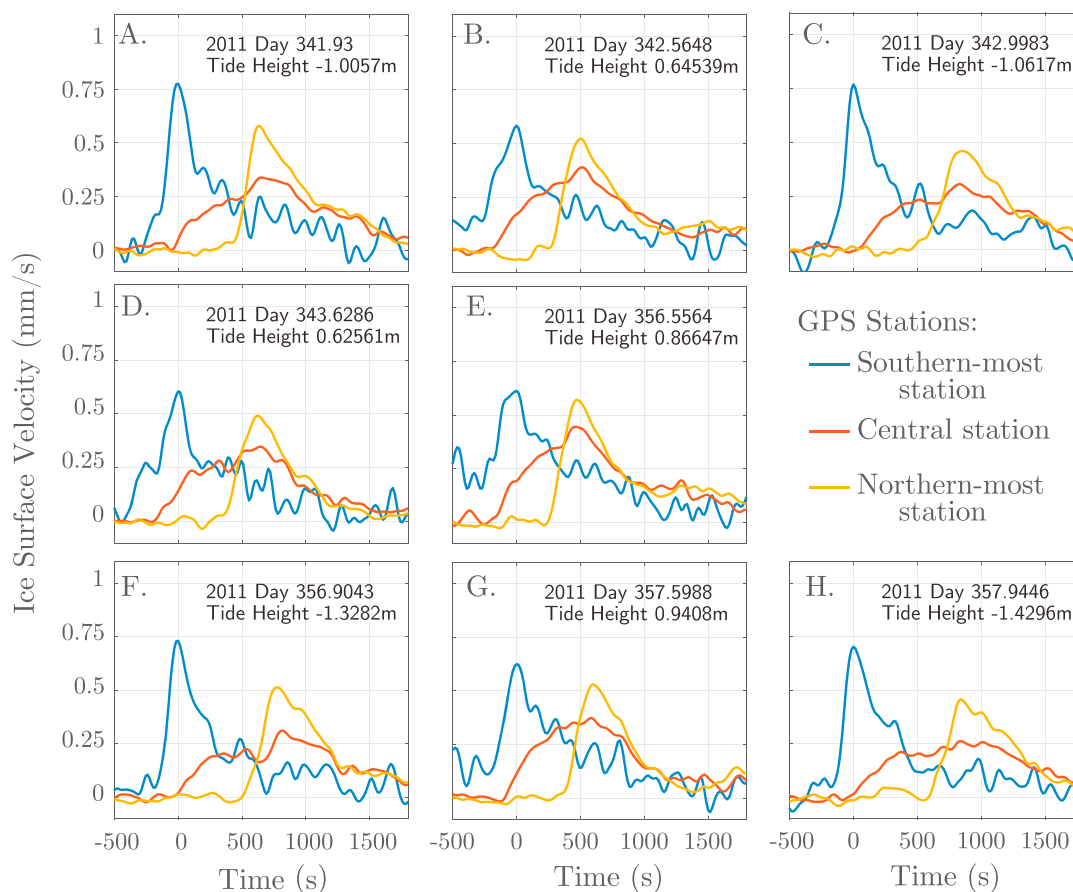


Figure 3. Eight spring tide slip events from the 2011 field season (colors correspond to stations shown in Figure 1). Time $t = 0$ corresponds to the instant of maximum slip rate at the southernmost (blue) station. Rupture propagates to the north.

and WIS to a much narrower several kilometers width near the Crary Ice Rise (CIR). The CIR is seen in the map in Figure 1 as the grounding zone peninsula that is the southwesternmost point of grounded ice shown in the map. The WIP is bounded to the south by the Engelhardt Ice Ridge and to the north by an inlet of the floating ice of the Ross Ice Shelf. The length of the WIP in the direction of flow varies from ~ 150 km near its northern boundary to ~ 300 km if a line is drawn from the MIS-WIS confluence to the tip of the CIR.

We focus on data from the December 2011 field season on the WIP [Winberry *et al.*, 2014a, 2014b]. The large spatial aperture (~ 80 km) of the GPS array at this time helps resolve details of the slip event rupture process. GPS station positions were recorded at 15 s intervals between 3 December and 23 December, and we low-pass filter these data below 60 s. During this 21 day period there were just under two fortnightly spring-neap tidal cycles and a total of 28 recorded slip events. We focus our analysis on the eight events during this time that occurred near periods of spring tide. Bindschadler *et al.* [2003] was the first to note that such events show a striking regularity in repeat time, slip amplitudes, and rupture style, making them ideal targets for modeling.

The timing of the WIP slip events is closely related to the tide height in the nearby ocean cavity beneath the Ross Ice Shelf [Bindschadler *et al.*, 2003]. We quantify these tides using the tide model of Padman *et al.* [2002] as plotted in Figure 2a. The subshef tides are dominated by diurnal components K_1 and O_1 . At the observation point nearest to the WIP (Site F9 in the study by Padman *et al.* [2002]), the four largest tidal constituents are the lunisolar diurnal constituent ($K_1 = 41$ cm), the principal lunar diurnal constituent ($O_1 = 40$ cm), the principal lunar semidiurnal constituent ($M_2 = 8$ cm), and the principal solar semidiurnal constituent ($S_2 = 11$ cm).

Two slip events per day occur during periods of spring tide (Figure 2). A typical tidal cycle tends to have its first slip event at or just after high tide and a second slip event about 9 h later, at or just before low tide. An approximately 15 h long period then separates this low tide event from the next high tide event. Events with

longer than 15 h recurrence period are commonly observed on the WIP. However, by focusing on the events that occur during spring tide, we exclude such events.

During a slip event, rupture typically initiates at the southern end of the WIP and propagates to the north [Walter *et al.*, 2011; Pratt *et al.*, 2014]. This propagation is illustrated in Figure 3, which plots the sliding velocity at three stations during eight slip events. Slip rate at the southernmost station (blue) accelerates about 500 s before acceleration of the northernmost station (yellow). These two stations are located 79.9 km apart, resulting in a rupture velocity ~ 160 m/s, an order of magnitude slower than the shear wave speed in ice. Between these two stations, the rupture has a decreased sliding velocity (red, central station). In section 7 we associate this diminished sliding velocity with rate-strengthening frictional properties in the central part of the WIP. Note also that at each location, acceleration occurs for about 200 s to peak slip rates ~ 0.4 – 0.8 mm/s. Deceleration then occurs over a much longer period of up to 15 min (Figure 3). The total amount of slip per event is ~ 0.5 m.

The ice of the WIP is underlain by a layer of subglacial till. The existence of this till layer has been inferred using seismic reflection studies [Bindschadler *et al.*, 1987] and has also been directly observed using hot water drilling [Kamb, 2001]. The till layer is generally thought to be up to several meters thick, water saturated, and clay rich [Tulaczyk *et al.*, 1998; Kamb, 2001]. In section 3.1.1 we present several important details concerning the mechanics of till deformation. First, we describe how this deformation fits in to our overall description of ice stream motion.

3. Model and Governing Equations

In this section, we present a model for an ice stream with rate-and-state friction at its bed. We introduce a coordinate system (Figure 1) with the positive x axis pointing in the downstream direction along a flow line, the y axis pointing in the transverse, cross-stream direction, and the z axis oriented vertically. For the region of the WIP that we consider, this corresponds to the x axis pointing approximately westward, the y axis approximately southward, and the z axis upward. The ice-bed interface is at $z = 0$, and the ice has uniform thickness $H = 800$ m. The center flow line of the WIP is located along $y = 0$. We assume that all motion occurs in the streamwise ($+x$) direction, with variation only in the cross-stream (y) direction; this leads to an antiplane strain problem (Figure 4a). Finally, we exploit the low aspect ratio, thin-layer nature of the geometry by depth-averaging the governing equations.

The depth-averaged momentum balance in the streamwise direction is

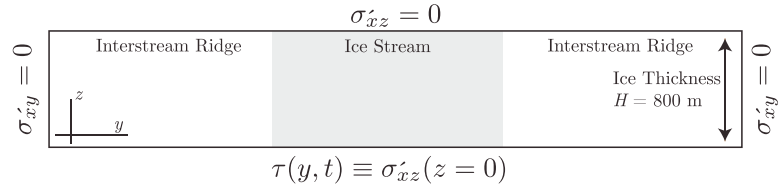
$$\rho \frac{\partial^2 u}{\partial t^2} = \frac{\partial \sigma_{xx}}{\partial x} + \frac{\partial \sigma_{xy}}{\partial x} - \frac{\tau}{H}, \quad (1)$$

where ρ is ice density and u is the streamwise displacement. The displacement u is assumed uniform with depth, which is consistent with scaling arguments for this thin-layer geometry. Furthermore, τ is the basal shear stress, and σ_{ij} are components of the depth-averaged stress tensor. Because ice is more compliant than rock, we neglect deformation of the bed material (below the till layer) and model ice sliding on an effectively rigid bed. Details regarding this assumption are provided in Appendix A.

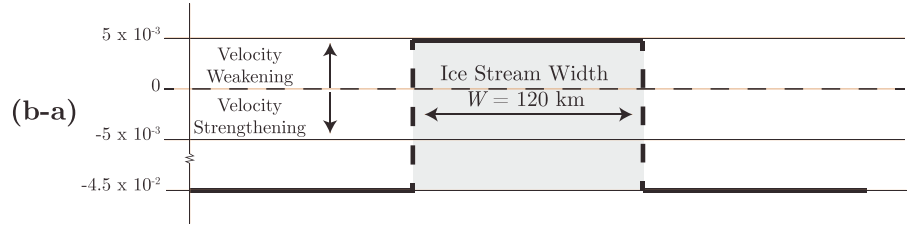
We have neglected the gravitational driving stress $\rho g H (-\partial S / \partial x)$, with gravitational acceleration g and ice surface height $S(x)$. The contribution of this term to the momentum balance is small because the ice surface gradient in the WIP, $(-\partial S / \partial x) < 25$ m over 150 km $\sim 10^{-4}$ [Fretwell *et al.*, 2013]. This gives $\rho g H (-\partial S / \partial x) < 1$ kPa, which is smaller than the other stresses in the momentum balance.

We treat ice as an elastic solid, neglecting ice viscosity based on the following analysis. In a viscoelastic material, viscous flow dominates elastic straining at timescales greater than the Maxwell viscoelastic relaxation time, $t_M \sim \mu / G$, for ice shear modulus G and viscosity μ . Ice has shear modulus $G = 3.6$ GPa [Vaughan *et al.*, 2016]. Ice viscosity μ depends on the effective strain rate $2\dot{\epsilon}_E^2 \equiv \dot{\epsilon}_{ij}\dot{\epsilon}_{ij}$ according to $2\mu = A^{-1/n} \dot{\epsilon}_E^{1/n-1}$ [Cuffey and Paterson, 2010]. Ice is shear thinning with $n = 3$. The rheology parameter $A = 24 \times 10^{-25} \text{ s}^{-1} \text{ Pa}^{-3}$ for temperate ice [Cuffey and Paterson, 2010], as expected at the bed of the WIP [Kamb, 2001]. Effective strain rates during a slip event are $\sim v_0 / (\sqrt{2}W) \sim 3 \times 10^{-9} \text{ s}^{-1}$, where $W \sim 120$ km is the ice stream width. Therefore, during a slip event, effective viscosity $\mu \approx 2 \times 10^{13} \text{ Pa s}$, giving an estimate of the relaxation time $t_M \approx 85$ min. Ice viscosity is thus negligible during slip events which last at most 30 min. Effective strain rates are approximately 24 times lower during loading, resulting in a viscosity that is larger by a factor ~ 8 . An elastic treatment of ice is therefore less justified during the stick phase. This view is supported by Winberry *et al.* [2014a], who provide

A. Model Geometry



B. Homogeneous Ice Stream Bed



C. Heterogeneous Ice Stream Bed

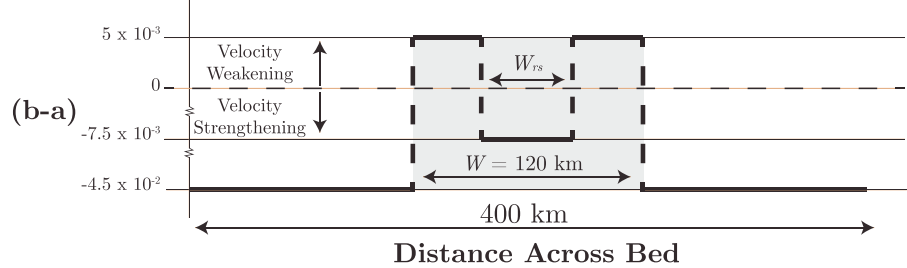


Figure 4. (a) Model geometry and (b and c) the distribution of frictional parameters used in this study. The prime symbol in Figure 4a denotes that the boundary conditions are enforced on the vertically resolved (as opposed to depth-averaged) stress components. Compare the dark shaded region in Figure 4a to the real WIP geometry in Figure 1.

observational evidence for the onset of viscous creep just prior to events with recurrence periods greater than $\sim 16 \text{ h}$. We recall from section 2, however, that no such events occur during the time period that we analyze in this study.

The components of the depth-averaged deviatoric stress tensor σ_{ij} are related to the components of the depth-averaged strain tensor ϵ_{ij} through Hooke's law. Assuming isotropic elasticity,

$$\sigma_{xx} = 2G \frac{1-\nu}{1-2\nu} \epsilon_{xx} \equiv G_* \epsilon_{xx} = G_* \frac{\partial u}{\partial x}, \quad (2)$$

where $\nu = 0.33$ is the Poisson ratio of ice [Vaughan *et al.*, 2016], and

$$\sigma_{xy} = G \epsilon_{xy} = G \frac{\partial u}{\partial y}. \quad (3)$$

Following Goldberg *et al.* [2014], we parameterize loading in the streamwise direction by approximating the longitudinal stress gradient as

$$\frac{\partial \sigma_{xx}}{\partial x} \approx \frac{\sigma_{xx}(x=L) - \sigma_{xx}(x=-L)}{L}, \quad (4)$$

where $L = 150 \text{ km}$ is the characteristic streamwise distance over which longitudinal compression occurs during a stick-slip cycle. The contribution at $x = -L$ introduces loading from the push of inflowing ice from the upstream direction. We assume a steady inflow velocity v_0 and approximate

$$\sigma_{xx}(x=-L) = G_* \epsilon_{xx} \approx G_* \frac{v_0 t - u}{L}. \quad (5)$$

At the downstream end, we assume that the longitudinal stress is due to a tidally varying hydrostatic pressure,

$$\sigma_{xx}(x=L, t) \equiv \sigma_{xx}^{\text{tide}}(t), \quad (6)$$

which is described in detail subsequently.

We combine the depth-averaged momentum balance equation (1), Hooke's law equations (2) and (3), and the longitudinal loading from equations (4) and (5) to arrive at

$$\rho \frac{\partial^2 u}{\partial t^2} - G \frac{\partial^2 u}{\partial y^2} = \frac{G_*}{L} \frac{v_0 t - u}{L} - \frac{\tau}{H} + \frac{\sigma_{xx}^{\text{tide}}}{L}. \quad (7)$$

3.1. Frictional Sliding

We use rate-and-state friction to describe the basal shear stress at the ice-till interface. We equate the basal shear stress τ to an evolving basal shear strength that is directly proportional to the effective pressure $\bar{\sigma}$:

$$\tau = f(v, \theta) \bar{\sigma}. \quad (8)$$

The friction coefficient $f(v, \theta)$ is a function of the sliding velocity $v \equiv \partial u / \partial t$ and a state variable θ that captures the history dependence of strength. The effective pressure $\bar{\sigma} = \rho g H - p$ for gravitational acceleration g and pore pressure p .

Whereas a traditional Coulomb-plastic friction model would have constant friction coefficient f , laboratory experiments show that f experiences slight variations as a function of sliding velocity. Under steady state sliding conditions, when sufficient slip has accumulated so as to erase any history dependence of strength, variations in the friction coefficient are typically proportional to the logarithm of the sliding velocity:

$$f_{ss}(v) = f_0 - (b - a) \log(v/v_0). \quad (9)$$

In this expression we have introduced the nominal coefficient of friction f_0 , which is defined as $f_{ss}(v_0)$. We have also introduced the frictional parameter $b - a$, which is defined as the rate of change of the steady state friction coefficient with logarithmic changes in sliding velocity,

$$-v \frac{df_{ss}(v)}{dv} \equiv (b - a). \quad (10)$$

Typical values of $(b - a)$ are of order 10^{-3} . When $b - a > 0$, an interface has less strength at faster sliding velocity and is called rate-weakening. When $a - b > 0$, an interface has more strength at faster sliding velocity and is called rate-strengthening.

Laboratory experiments additionally show transient strength changes that occur before steady state conditions are reached. During a step increase in sliding velocity, this transient strength change takes the form of an instantaneous strengthening, termed the direct effect. The amplitude of the strength increase due to the direct effect defines the friction rate parameter a as the rate of change of the instantaneous value of the friction coefficient with logarithmic changes in sliding velocity,

$$v \frac{\partial f(v, \theta)}{\partial v} \equiv a. \quad (11)$$

Typical values of a are of order 10^{-3} . This transient strengthening is essential to ensure mathematical well-posedness in the sense described by *Rice et al.* [2001].

The two effects quantified by equations (10) and (11) are described within the friction constitutive law as [*Dieterich, 1979; Ruina, 1983; Rice and Ruina, 1983; Marone, 1998; Rice et al., 2001; Dieterich, 2007*]

$$f(v, \theta) = f_0 + a \log\left(\frac{v}{v_0}\right) + b \log\left(\frac{v_0 \theta}{d_c}\right). \quad (12)$$

The second term on the right-hand side of equation (12) describes the direct effect, and the third term describes state evolution.

We must additionally specify an evolution law for the state variable θ that describes how the friction coefficient $f(v, \theta)$ in equation (12) achieves its steady state value. In this study, we choose the aging law,

$$\frac{\partial \theta}{\partial t} = 1 - \frac{v \theta}{d_c}, \quad (13)$$

which introduces the state evolution distance d_c as the characteristic slip distance over which f approaches f_{ss} . The state evolution law (equation (13)) shows that the friction coefficient increases proportional to the logarithm of time during periods of low sliding velocity ($v \theta / d_c \ll 1$) [*Dieterich, 1972*]. Several other choices of evolution law are available [*Marone, 1998; Rice et al., 2001; Dieterich, 2007; Ampuero and Rubin, 2008*], but we have verified that the major conclusions of this paper are independent of the choice of evolution law.

3.1.1. The Mechanical Basis of Rate-and-State Friction

The two principal behaviors that are described by rate-and-state friction, an instantaneous friction increase during velocity steps (equation (11)) and evolution to a velocity-dependent steady state friction coefficient over a characteristic amount of sliding d_c (equation (10)), occur for a wide range of frictional interfaces and may be due to many different physical processes. For this reason, we envision rate-and-state friction as a class of sliding behavior rather than as any one particular physical process. We briefly review the mechanical basis of several glaciological processes that fit within the rate-and-state framework.

Rate-and-state friction was originally formulated to explain friction in rocks at low homologous temperature, and recent laboratory results suggest that this setting is comparable to that of ice sliding against rock in the low homologous temperature limit [McCarthy *et al.*, 2017]. In this setting, the direct effect (equation (11)) is thought to be due to thermally activated creep at asperity contacts [Nakatani, 2001]. The aging effect (equation (10)) is thought to be due to the growth of asperity contacts during periods of stationary (or near-stationary, i.e., $v/v_0 \ll 1$) contact [Dieterich and Kilgore, 1994]. Additional thermal effects may also be important [Rice, 2006; McCarthy *et al.*, 2017], and a complete review of this topic is beyond the scope of this paper. We do, however, note one important phenomenon concerning the sliding of ice against rock. In this setting, friction transitions from rate-weakening to rate-strengthening behavior as temperatures rise above -15°C . This transition may occur due to the onset of pressure melting at highly stressed microscopic asperity contacts, although further work is necessary to confirm this hypothesis [McCarthy *et al.*, 2017]. This mechanism for rate-weakening friction seems unlikely to occur on the WIP, however, due to the WIP having basal temperature near the pressure melting point [Kamb, 2001].

Ice stream sliding generally occurs in regions where the ice sheet bed is composed of glacial till. As a fluid-saturated granular material, till bears some similarity to the fault gouges typically found along tectonic faults. The accumulation of granular wear products along sliding interfaces is a stabilizing process, i.e., a process that favors velocity strengthening friction [Byerlee, 1967; Marone *et al.*, 1990]. This stabilization is due to dilation of the granular material and has been observed during laboratory experiments on glacial tills [Rathbun *et al.*, 2008; Rathbun and Marone, 2010]. This dilation results in contributions to both the frictional direct and aging effects [Marone *et al.*, 1990], although we do not directly account for this dilation in this study.

Additional processes that occur during the shearing of glacial till may, however, result in rate-weakening behavior. In particular, particle ploughing is a phenomenon that occurs during shearing of fluid-saturated granular materials with a nonhomogeneous grain size distribution [Thomason and Iverson, 2008; Iverson, 2010]. Under shear, a region with elevated pore pressure forms in front of anomalously large granular particles. This process is rate weakening. Particle ploughing was not observed by Rathbun *et al.* [2008] and Rathbun and Marone [2010]; however, this is likely due to the fact that the sheared samples in these studies had large grains (>1 mm) removed, thereby removing the grain size heterogeneity required for particle ploughing.

Although the WIP rests on a bed composed of glacial till, we note here that rate-and-state friction is also applicable to glacier sliding in the absence of glacial till. Ice flowing over a nonplanar, rigid bed tends to form cavities in the downstream or leeward side of bedrock protrusions. At higher velocities these cavities grow in size. This loss of contact between the ice and the bed results in reduced shear resistance. This process of cavitation has been shown to have rate dependence and to show evolution toward a steady state in both theory [Lliboutry, 1968; Schoof, 2005] and experiments [Zoet and Iverson, 2015, 2016].

3.1.2. Parameter Choices

We use frictional parameters (Table 1) in our simulations that are consistent with experimentally determined values [Thomason and Iverson, 2008; Rathbun *et al.*, 2008; Rathbun and Marone, 2010; Schulson and Fortt, 2012; Zoet *et al.*, 2013; McCarthy *et al.*, 2017]. We use $a = 0.02$ and $b - a = 0.005$ in rate-weakening regions. In section 7, we examine the effect of a rate-strengthening region, and in this region we use $a = 0.02$ and $a - b = 0.0075$. These values are consistent with values reported in the literature where a falls in the range $0.01 - 0.1$ and $|a - b|$ falls in the range $0.001 - 0.02$. In this study, we do not vary the parameters a and $b - a$ from the values listed in Table 1.

Appropriate values for the state evolution distance d_c are less certain. Few studies report values of the state evolution distance d_c , and reported values vary over several orders of magnitude. In low homologous temperature sliding between two materials, d_c is thought to scale with material grain size [Rice *et al.*, 2001]. However, when granular material is present along the interface, Marone *et al.* [1990] has shown that d_c varies with the width of shearing within this layer. For rate-strengthening granular layers, this width of shearing may grow

Table 1. Table of Parameters

Quantity	Symbol	Unit	Value
Ice shear modulus	G	GPa	3.6
Ice density	ρ	kg/m ³	916
Ice Poisson ratio	ν		0.33
Ice shear wave speed	c	m/s	2000
Nominal friction coefficient	f_0		0.4
Inflow velocity	v_0	m/s	10 ⁻⁵
Direct effect parameter	a		2 × 10 ⁻²
Healing parameter, rate-weakening	b_{rw}		2.5 × 10 ⁻²
Healing parameter, rate-strengthening	b_{rs}		1.5 × 10 ⁻²
Ice thickness	H	m	800
Stream wise loading distance	L	km	150
Width of grounded ice	W	km	120
Width of the computational domain		km	200
Width of rate-strengthening zone	W_{rs}	km	variable
Effective pressure	$\bar{\sigma}$	kPa	variable
State evolution distance	d_c	m	variable

to the width of the entire granular layer. For rate-weakening materials, however, shearing localizes to a much narrow width [Marone *et al.*, 1990]. The meter-scale till thickness inferred to exist beneath the Antarctic ice streams [Bindschadler *et al.*, 1987] is therefore not necessarily expected to be informative of the width of shear deformation or of d_c . In contrast, in the context of a rigid ice-bed interface, Figure 3 in the work of Zoet and Iverson [2016] shows a shear stress evolution consistent with $d_c \sim 1.5$ m. Because of this order of magnitude uncertainty, we treat d_c as a free parameter and tune its value to match conditions observed on the WIP.

3.2. Tidal Forcing

In this section we incorporate the effects of tidal stress variations. A longitudinal stress gradient at the grounding line arises due to the difference in the hydrostatic pressure in the grounded and floating ice [Goldberg *et al.*, 2014]. The expression for the resulting stress, $\sigma_{xx}^{\text{tide}}$, is given as equation (2) in Goldberg *et al.* [2014],

$$\sigma_{xx}^{\text{tide}} = \rho g H - \frac{\rho_w g}{H} \left(\frac{\rho}{\rho_w} H + H_{\text{tide}} \right)^2. \quad (14)$$

We note here that other ice stream stresses may experience tidal modulation in addition to the hydrostatic pressure. Several studies have suggested that other types of tidal loading may influence tidally modulated ice stream flow including flexural, buttressing, and basal shear strength [Minchew *et al.*, 2016; Walker *et al.*, 2013; Sayag and Worster, 2013; Rosier *et al.*, 2014; Rosier and Gudmundsson, 2016]. Within our cross-stream force balance approximation, many of these loading geometries are inaccessible. We do, however, discuss possibilities for incorporating additional loading in our model in section 8.

Throughout this study, we prescribe a tide with maximum amplitude $H_0 = 1$ m with diurnal period $T_{\text{tide}} = 24$ h,

$$H_{\text{tide}}(t) = H_0 \sin \left(\frac{2\pi t}{T_{\text{tide}}} \right). \quad (15)$$

This tidal forcing is independent of the cross-stream coordinate y and is a simplification of the actual tidal forcing that consists of multiple tidal constituents with varying phase, spatial pattern, and amplitude. The tidal parameters are chosen to reflect typical WIP grounding zone tides during a spring tide period and are consistent with the best available Ross Ice Shelf tide model [Padman *et al.*, 2002].

When the tidal height change is much less than the buoyancy height $(\rho/\rho_w)H$, then the tidal forcing is approximately

$$\sigma_{xx}^{\text{tide}}(t) \approx \rho g H \left(1 - \frac{\rho}{\rho_w} \right) - 2\rho g H_{\text{tide}}(t). \quad (16)$$

This approximation is used hereafter. We will later see that tidal modulation is more sensitive to stressing rate than to absolute stress. For this reason we note that the tidal stressing rate, within the small tide limit, is

$$\frac{d\sigma_{xx}^{\text{tide}}}{dt} = -2\rho g \frac{dH_{\text{tide}}}{dt}. \quad (17)$$

In the following sections we describe the variety of sliding solutions that can arise from these governing equations.

4. Stability of Steady Sliding

Rate-and-state friction, when coupled to an elastic solid that is loaded at a steady rate, can give rise to both steady sliding and stick-slip cycles, depending on the elastic compliance of the system, friction parameters, and effective pressure. The transition between these two sliding styles is readily quantified using a linear stability analysis to study the behavior of small, spatially periodic perturbations about the steady sliding solution [e.g., *Rice and Ruina, 1983; Rice et al., 2001*]. We present a linear stability analysis for the thin-layer geometry unique to WIP in Appendix B1 and summarize pertinent results here. Periodic tidal forcing is neglected throughout this discussion.

Steady sliding occurs when perturbations of all wavelengths decay in time, so the interface returns to a state of steady sliding. Sliding is always stable for rate-strengthening friction ($a - b > 0$) and conditionally stable for rate-weakening friction ($b - a > 0$). Rate-weakening behavior is thus a necessary condition for stick-slip.

For rate-weakening friction, short wavelength perturbations decay and long wavelength perturbations grow in time. The critical wavelength at neutral stability is interpreted, in an approximate manner, as twice the critical ice stream width W_c , leading to the condition for instability in terms of ice stream width W

$$W > W_c \equiv \pi \sqrt{\frac{HGd_c}{\bar{\sigma}(b-a)}}. \quad (18)$$

This expression for W_c neglects inertia and the stiffness of the system in the streamwise direction; the general expression is provided in Appendix B1. Since W is fixed in our description, equation (18) may be rearranged so as to emphasize the dependence on effective pressure $\bar{\sigma}$, which must exceed a critical value $\bar{\sigma}_c$ for instability:

$$\bar{\sigma} > \bar{\sigma}_c \equiv \frac{\pi^2 HGd_c}{W^2(b-a)}. \quad (19)$$

The conditions in equations (18) and (19) are strictly valid for infinitesimally small perturbations, but numerical simulations of the nonlinear equations, as well as analytical analyses of nucleation [*Viesca, 2016a*], demonstrate that stick-slip cycles arise when these conditions are satisfied. A more precise condition under which stability (equation (18)) is unaffected by inertia is derived in Appendix B2.

When $W \gg W_c$, slip events take the form of ruptures that propagate across the ice stream at a speed close to the shear wave speed in ice. In contrast, close to neutral stability ($W \approx W_c$), the system response takes the form of slow-slip events. The linearized analysis shows purely oscillatory response at neutral stability, with oscillations having period

$$T_c \equiv 2\pi \sqrt{\frac{a}{b-a} \frac{d_c}{v_0}}. \quad (20)$$

Note that T_c is independent of effective pressure and directly proportional to d_c . We later show that T_c provides a reasonably accurate prediction of recurrence period close to neutral stability, even for the nonlinear equations, and we use this to constrain d_c after making some assumptions regarding the value of a/b (since v_0 is fairly well known).

The discussion in this section has focused on a linear stability analysis and so has neglected nonlinear effects. In order to analyze the evolution of slip and stress throughout an entire stick-slip cycle, we turn in the following sections to the use of numerical simulations.

5. Ice Stream Motion Without Tidal Forcing

We now examine sliding style as a function of the parameter W/W_c in the absence of tidal forcing. We numerically solve the nonlinear system of equations (7), (12), and (13) for an ice stream with width $W = 120$ km. We take the ice stream bed to have constant rate-weakening properties beneath it (Figure 4b), but in a later section we explore spatially heterogeneous frictional properties in order to better match the GPS time series.

Our numerical domain is 400 km wide which is sufficiently wide so that solutions are independent of this particular size. The ice stream is centrally located within this larger domain (Figure 4). The complement of the central ice stream region consists of two boundary regions that each have width $(400 \text{ km} - W)/2 = 140$ km and intensely rate-strengthening friction ($a - b = 0.045$). This choice represents a compromise between the appropriate boundary condition for the part of WIP that is bordered by an interstream ridge and the appropriate boundary condition for the part that is bordered by floating ice (section 2). Our cross-stream ice model is not capable of describing flow line variation in any longitudinally oriented boundary condition, and so a more realistic boundary is not possible at this point. This parameterization, however, does have several useful features. Because the part of the WIP that is shown in Figure 1 is bounded by floating ice, it likely experiences loading from the floating ice that surrounds it. This type of loading does occur in our model because the boundary regions in our simulations experience nearly steady sliding. In all of our simulations, the computational domain is terminated with zero traction lateral boundary conditions ($\partial u / \partial y = 0$). These boundary conditions permit continual advance of the ice, even with an ideally elastic rheology that does not allow permanent deformation. More details concerning our numerical method is provided in Appendix C.

When $W/W_c \lesssim 1$, sliding is steady and the sliding velocity is equal to the loading velocity v_0 . In contrast, stick-slip cycles occur when $W/W_c \gtrsim 1$, with slow slip occurring just above neutral stability. A complete stick-slip cycle consists of a stick phase and a slip event, the latter consisting of a nucleation phase, a phase of high slip velocities (and inertially limited rupture, at least when $W/W_c \gg 1$), and a phase of deceleration. The linear stability analysis provides only approximate conditions for instability of a finite-width system, which is reflected in our use of the symbols \lesssim and \gtrsim in this discussion.

Ice inflow loads the WIP. If the WIP experiences zero slip in the time between slip events, then the momentum balance (equation (7)) sets this loading rate to be

$$\dot{\tau} = G_* \frac{H v_0}{L}. \quad (21)$$

The recurrence period T is equal to the time required to load the WIP to a stress level equal to the stress drop in a slip event, $\Delta\tau$:

$$T \sim \frac{\Delta\tau}{\dot{\tau}}. \quad (22)$$

This relation describes the type of sliding where all accumulated stress is relieved through periodic slip events and would require modification if viscous stress relaxation were to occur.

In general, the slip event stress change $\Delta\tau$ and therefore the recurrence time T are nonlinear functions of the frictional and elastic properties of the ice stream. In Appendix B1, however, we show that the recurrence period near neutral stability follows the simple relation,

$$\frac{T}{T_c} \approx \frac{W}{W_c}, \quad (23)$$

where T_c is given by equation (20). We verify that the slow-slip limit matches this scaling in Figure 5b.

This expression for the recurrence time in the slow-slip limit (equation (23)) is useful because it describes the recurrence time for the style of sliding most similar to the observed behavior of the WIP. Equation (23) shows that the recurrence time reaches a minimum at neutral stability. This result suggests that the pattern of increasing recurrence times over the last decade of observations on the WIP are consistent with increased effective pressure $\bar{\sigma}$ and a transition to more unstable conditions. We discuss this point further in section 8.2.

The evolution of sliding velocity during nucleation and rupture are shown in Figure 6 for two values of W/W_c (with W_c altered by varying the effective pressure $\bar{\sigma}$). During nucleation, slip accelerates in a region of the bed of size equal to the critical width W_c . Close to neutral stability ($W/W_c = 1.1$, Figures 6a and 6c), nucleation occurs over a long duration (~ 500 s for this example) and all slip occurs at relatively small sliding rate

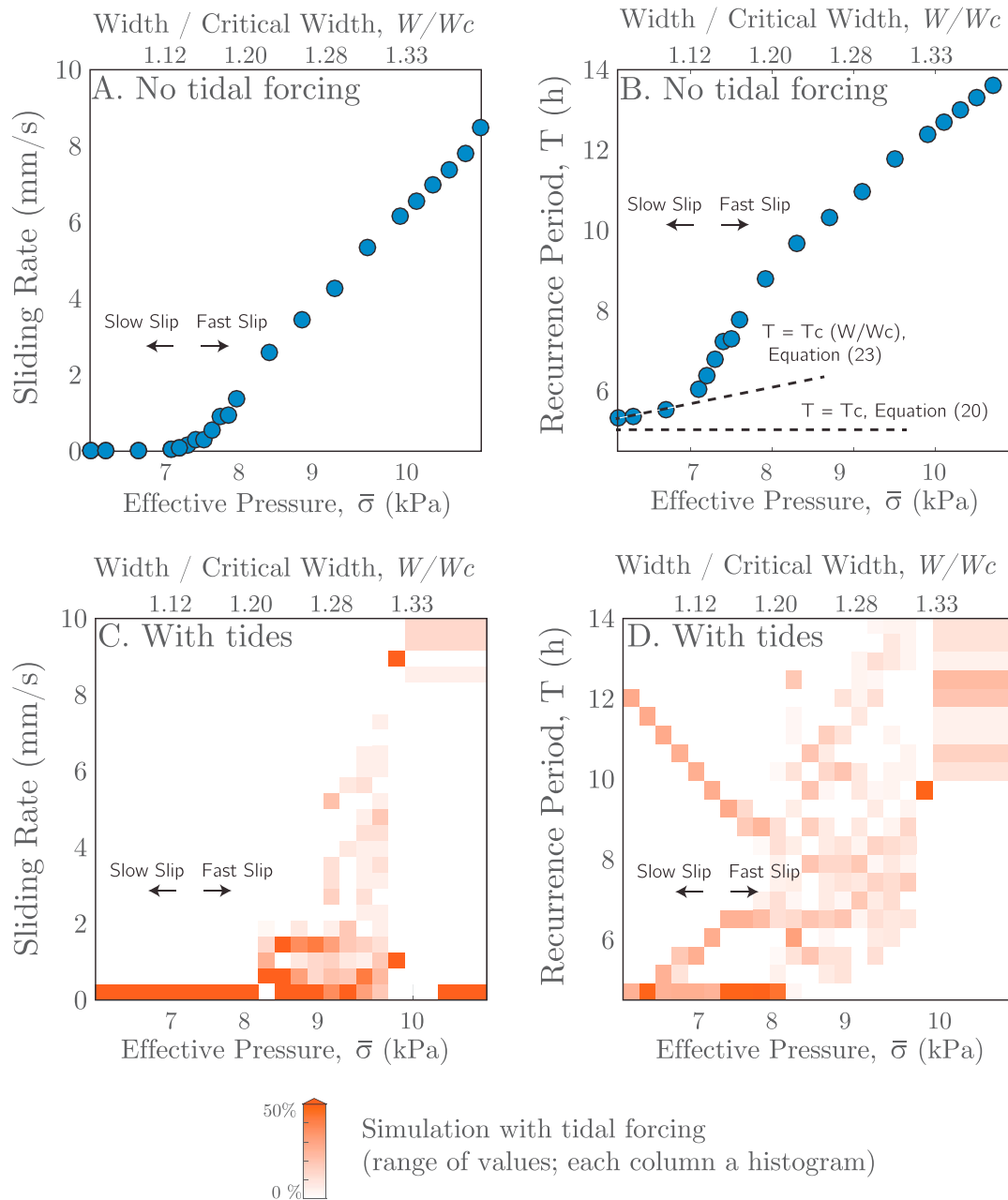


Figure 5. (a and c) Maximum sliding rates during slip events and (b and d) recurrence periods for a range of effective pressures $\bar{\sigma}$. Although the maximum sliding rate varies with effective pressure $\bar{\sigma}$, the long-term average sliding rate is constant and equal to the loading velocity v_0 . All simulations have $d_c = 14$ mm. When tidal forcing is absent (Figures 5a and 5b), all slip events are identical and periodic. When tidal forcing is present (Figures 5c and 5d), slip events occur with a range of maximum sliding rates and recurrence periods. In Figures 5c and 5d, each column is a histogram whose values saturate at 50%. Several simulations from this figure are shown in Figure 8.

with negligible effects of inertia. This is a slow-slip event, so called because of their characteristically low maximum sliding rates, as plotted in Figure 5a. We emphasize, however, that although the maximum sliding rate is a function of W_c , the cycle-averaged velocity remains constant in our model and equal to the loading velocity v_0 .

Further from neutral stability ($W/W_c = 2.0$, Figures 6b and 6d), nucleation occurs more rapidly (~ 50 s for this example), during which only a small amount of the total slip has accumulated. Most slip occurs later, following a rupture front that propagates at nearly the shear wave speed across the interface and carries with it a localized stress concentration that brings the interface to failure. This is a fast-slip event or rupture. For the setup

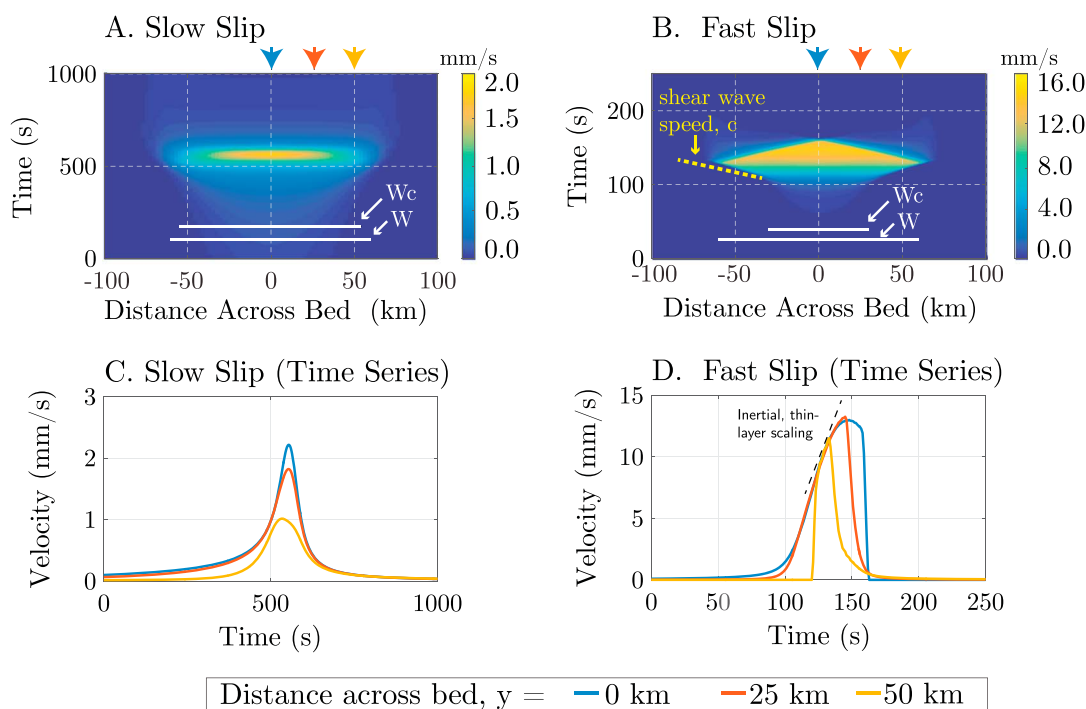


Figure 6. (a and b) Space-time diagrams and (c and d) velocity time series for slip events in the slow-slip ($W/W_c = 1.1$, Figures 6a and 6c) and fast-slip ($W/W_c = 2.0$, Figures 6b and 6d) limits. Note the different axes in the two columns. The time series are from three locations across the ice stream, marked in corresponding colors at the top of the space-time diagrams.

shown here, the rupture expands until it reaches the rate-strengthening boundaries of the ice stream. Rapid sliding is inhibited in this region, so the rupture arrests. However, inertia of the ice sends a shear wave, known as an arrest wave, back across the ice that transmits a stress change that halts rapid sliding [Madariaga, 1976]. When the arrest wave reaches the center of the fault, the slip event is over; its duration is therefore approximately equal to the two-way travel time of a shear wave from the center of the rate-weakening region to the boundary between rate-strengthening and rate-weakening material and back again, $\sim W/c$.

We also point out an inertial scaling relation that is unique to the thin-layer geometry of ice streams. In the usual tectonic setting, where the fault is bounded by effectively semi-infinite elastic blocks, a stress drop $\Delta\tau$ leads to a slip velocity $v \sim \Delta\tau/(2\rho c)$, where ρc is the shear wave impedance. This so-called radiation-damping response arises from the outward radiation of elastic waves from the fault [Rice, 1993] that accelerate an increasing volume of the solid surrounding the fault following the wave arrival. In contrast, in the thin-layer geometry waves are reflected from the free surface back to the fault (or ice sheet bed), so that the region experiencing stress change has finite extent H in the direction normal to the interface. This leads to a constant slip acceleration $a \equiv \partial v/\partial t \sim \Delta\tau/(2\rho H)$ rather than constant slip velocity. This scaling is shown in Figure 6d with a dashed line, and we have verified its accuracy for many other fast-slip rupture simulations.

Although fast slip is frequently observed in the context of tectonic earthquakes, observational evidence for such behavior in ice sheets, at spatial scales comparable to or larger than the ice sheet thickness, is limited. One possible case where such high rupture velocities may occur is the family of repeating slip events that occur on the David Glacier, East Antarctica [Zoet et al., 2012]. The magnitude of slip events on the David Glacier are only constrained by regional seismic data. From these data, it is unclear whether the description of large-scale sliding that we have developed here is appropriate. Another possibility, for example, is that the region of the David Glacier bed experiencing rapid slip is in the $W \ll H$ limit, in which case it may be more appropriate to neglect free surface effects [Lipovsky and Dunham, 2016]. We further discuss this point in section 8.3.

6. Tidally Forced Ice Stream Motion

Sliding behavior exhibits a range of styles in the presence of tidal forcing. We explore the ice stream response to tidal forcing by varying two nondimensional parameters. First, we vary the critical width in relation to the

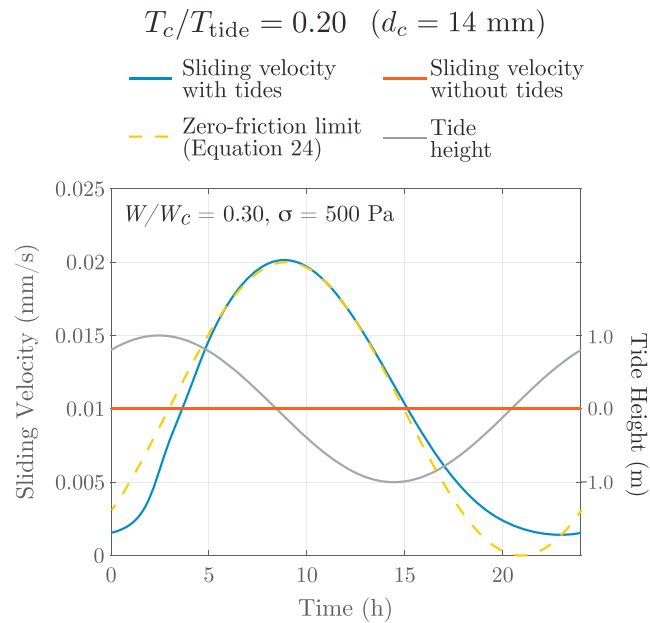


Figure 7. Quasi-steady tidally modulated ice stream centerline sliding velocity (blue) and tidal height (gray). Without tidal forcing, sliding would be steady (red).

ice stream width, W/W_c , by varying the effective pressure $\bar{\sigma}$. We find that when $W/W_c \gtrsim 1$, tidally modulated stick-slip cycles occur and when $W/W_c \lesssim 1$, tidal stresses modulate the sliding velocity, but stick-slip oscillations do not occur. We refer to the latter type of behavior as quasi-steady tidal modulation and note that it has been observed at many ice streams [Anandakrishnan et al., 2003; Gudmundsson, 2006; Marsh et al., 2013; Minchew et al., 2016]. Both of these behaviors arise naturally from our model.

Second, we vary the ratio of the tidal period to the frictional timescale, T_c/T_{tide} , by varying d_c . When $T_c/T_{\text{tide}} \ll 1$ many slip events occur per tidal cycle. In the opposite $T_c/T_{\text{tide}} \gg 1$ limit, many tidal cycles occur between slip events. The WIP has two slip events per tidal cycle and therefore lies between these two limits. By varying both W/W_c and T_c/T_{tide} , we successfully reproduce the timing of the WIP slip events.

A third dimensionless parameter that is not explored in our study is the amplitude of the tidal forcing relative to the slip event stress drop, $\rho g H_{\text{tide}}/\Delta\tau$. We note, however, that $\rho g H_{\text{tide}}/\Delta\tau \sim (18 \text{ kPa}/1 \text{ kPa}) = 18$ for the WIP events. The tides provide a remarkably large forcing at WIP, exactly the opposite of the situation typically encountered for tectonic earthquakes where tidal stress changes are vastly smaller than earthquake stress drops.

6.1. Quasi-Steady Tidally Modulated Sliding

Tidally modulated sliding without stick-slip is shown in Figure 7 ($W/W_c = 0.3$). Without tidal forcing, the ice stream would exhibit steady sliding (red line), but tidal forcing introduces perturbations about this steady sliding velocity (blue line). The maximum sliding rate occurs during times of falling tide (Figure 7). This occurs because a falling tide alters the basal shear stressing rate with the sign that favors accelerated sliding velocity. In the extreme limit where frictional and elastic effects are negligible, the dominant balance in the momentum balance equation (7) is between loading and tidal modulation. In this limit, the sliding velocity varies around v_0 as

$$v = v_0 - \frac{\rho g L}{G * T_{\text{tide}}} \cos\left(\frac{2\pi t}{T_{\text{tide}}}\right). \quad (24)$$

Equation (24) predicts the 90° phase shift between tidal forcing and sliding velocity.

This style of quasi-steady tidally modulation has been observed, for example, on the Bindschadler Ice Stream by Anandakrishnan et al. [2003]. In particular, Anandakrishnan et al. [2003] observed a 90° phase shift between tidal forcing and sliding velocity (compare, for example, their Figure 3). Simulations further confirm this style of tidal modulation, as shown in Figure 7. We note that a more general approach to this problem would be to add

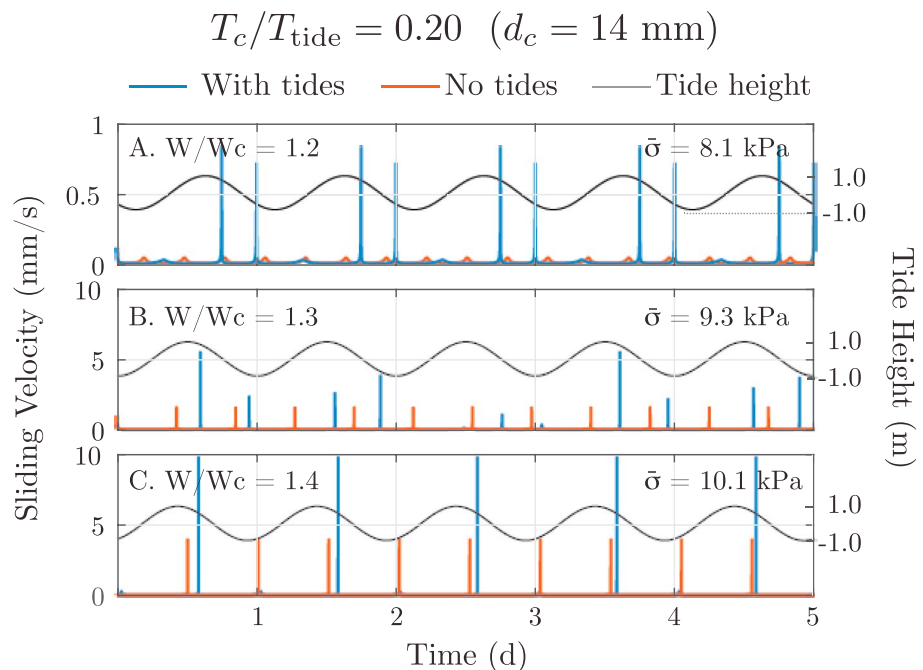


Figure 8. (a) When $d_c = 14 \text{ mm}$, two slip events occur per day with sliding velocities that match those observed on the WIP (compare to Figures S1 and S2 in the supporting information). (b and c) Simulations with increased effective pressure $\bar{\sigma}$. Although the maximum sliding rates increase with increasing $\bar{\sigma}$, the time-averaged sliding rates remain equal to the loading rate v_0 .

periodic forcing directly to the linearized governing equations to determine the transfer function between the forcing and velocity perturbation, but we defer such analysis to future work.

6.2. Tidally Modulated Stick-Slip Cycles

Tidally modulated stick-slip cycles occur when $W/W_c \gtrsim 1$, and these cycles have many similarities to the cycles that occur without tidal modulation. As in the case without tidal modulation, maximum slip event sliding rates and recurrence times are an increasing function of W/W_c (Figures 5c and 5d). The most pronounced difference between ice stream motion with and without tides is the tendency for slip events to occur during periods of falling tide. This modulates both slip event sliding rates and recurrence times.

We focus here on values of T_c/T_{tide} that give rise to two slip events per day in order to match the WIP event timing. This behavior emerges when $T_c/T_{\text{tide}} = 0.2$ and $W/W_c = 1.2$ (Figure 8a). In the supporting information we present additional simulations where many events occur per tidal cycle (supporting information Figure S1) and also where many tidal cycles occur between each slip event (Figure S2). Figure 8b shows that complex patterns of slip may result from our model. Although future studies may wish to explore this behavior in greater depth from a dynamical systems point of view [e.g., *Balanov et al., 2009*], we instead focus here on simulations that bear closer resemblance to the WIP observations.

Negative longitudinal stress rates during periods of rising tide inhibit slip events. This effect can be understood by examining the combined longitudinal stresses due to ice inflow and tidal forcing, as shown in Figure 9a. Note that this is the same simulation as shown in Figure 8a. Figure 9a plots the leftmost and rightmost terms from the right-hand side of the momentum balance (equation (7)). Considering only the effect of this altered stressing rate and neglecting any tidal influence on the slip event stress drop, we predict a modification to the rate of basal shear stress accumulation (equation (21)), as

$$\begin{aligned} \dot{\tau} &= -G_* \frac{H}{L} \frac{v_0}{L} + \dot{\sigma}_{xx}^{\text{tide}} \\ &\approx -G_* \frac{H}{L} \frac{v_0}{L} - 2\rho g H_0 \cos\left(2\pi \frac{t}{T_{\text{tide}}}\right). \end{aligned} \quad (25)$$

In writing this expression we have assumed small tidal heights (equation (17)) and daily tidal periods (equation (15)). Using equation (25) with the expression for the recurrence time (equation (22)) then demonstrates that the recurrence time should increase during times of rising tide because $\dot{\sigma}_{xx}^{\text{tide}} < 0$. For the simulation

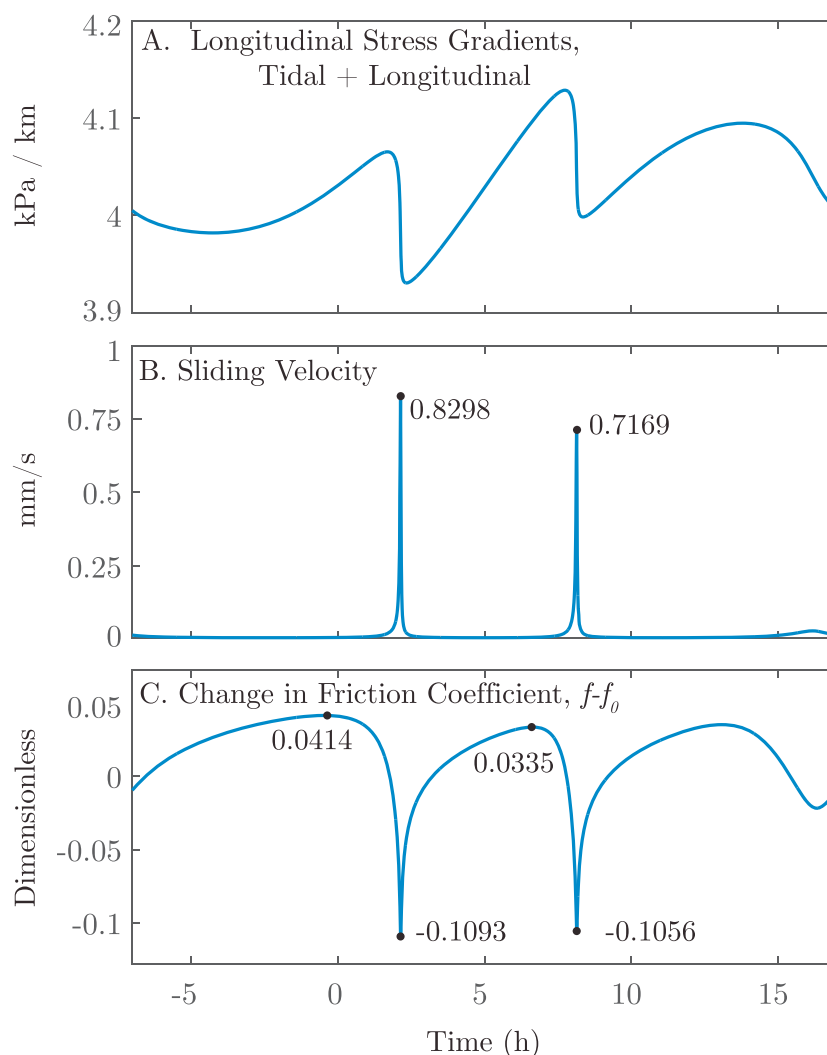


Figure 9. During a slip event there is a rapid decrease in (a) the longitudinal stress gradient, which consists of the sum of loading from ice inflow and tidal loading terms from the momentum balance equation (7). This stress change results from (c) the drop in the friction coefficient and results in (b) elevated sliding velocities. The corresponding velocity time series is shown in Figure 8a. Figure 9a is comparable to Figure 1 in *Savage and Marone* [2007].

shown in Figure 8a and Figure 9, this increase in the recurrence period is sufficiently long that no large slip events occur during times of rising tide.

Although no large slip events occur during rising tide, our simulations with two slow-slip events per day do predict the existence of a muted, third event during this time. This muted event occurs during a period of rising tide but is suppressed by the unfavorable stress state. The muted event can be seen in the time series in Figure 8a. The muted event is shown more clearly in Figure 10, which plots a phase portrait of the friction coefficient and the sliding velocity throughout a tidal cycle. Phase portraits for additional simulations are shown in supporting information Figure S3.

Slip events tend to occur during periods of peak stressing rate as opposed to periods of peak stress. This result is consistent with previous experimental and numerical studies [Beeler and Lockner, 2003; Savage and Marone, 2007; Ader et al., 2014]. Beeler and Lockner [2003] showed that this response is typical of frictional sliding in the limit that oscillatory forcing has a much greater period than the unforced recurrence time (their Figure 6b). We also note the similarity between our Figure 9a and Figure 1, left inset of *Savage and Marone* [2007]. However, these previous studies did not study tidal forcing with as large an amplitude relative to the slip event stress drop as occurs on the WIP.

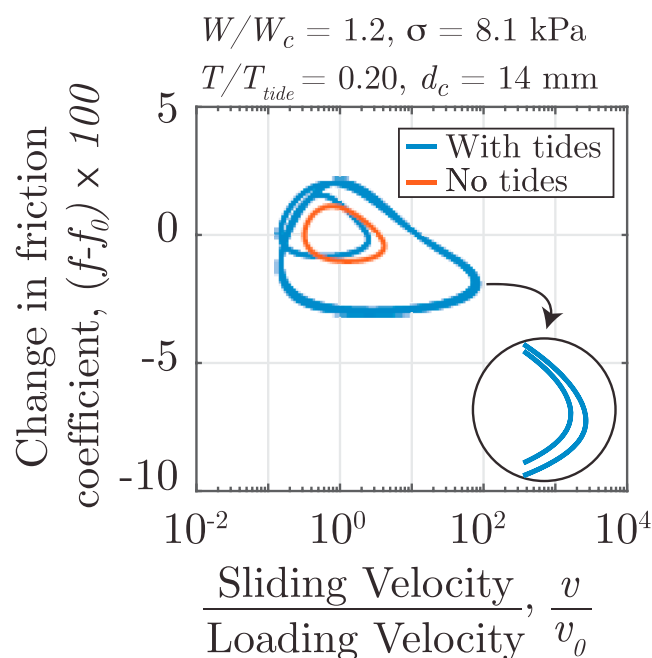


Figure 10. Friction-velocity phase portrait for the simulation shown in Figure 8a and Figure 9. The blue curve shows the phase portrait for a simulation with tidal forcing, and the red curve shows the phase portrait for the same simulation but without tidal forcing. Additional phase portraits are shown in the supporting information. Steady sliding occurs at the point where $f = f_0$ and $v = v_0$.

Tidal modulation also affects the basal shear strength change during a slip event. This effect occurs because the inhibition of slip events results in a longer recurrence period and therefore allows the bed to experience additional strengthening. This additional strengthening is apparent in Figure 9c, which plots changes in the friction coefficient throughout a tidal cycle. This figure shows that the coefficient of friction reaches its greatest value, $f - f_0 = 0.0414$, near the time of high tide. The change in the friction coefficient for the larger, high tide slip event is then 0.1507 but only 0.1391 for the smaller, low tide event.

7. Heterogeneous Bed Properties

We have so far assumed, for simplicity, that the bed is spatially homogeneous. While this assumption is adequate to develop an understanding of conditions for slow slip and tidal modulation, it produces perfectly symmetric slip events that nucleate from the center of the ice stream before spreading bilaterally. This type of symmetric, bilateral rupture is shown, for example, in the slow-slip event plotted in Figure 6c. However, as discussed in section 2, slip events on the WIP are not symmetric. Instead, WIP slip events show a clear sense of rupture propagation with the southernmost portion of the ice stream sliding several hundred seconds before the onset of sliding at the opposite, northernmost end of the ice stream (see Figure 3). In this section we demonstrate that this style of unilateral rupture propagation arises in our ice stream model when the ice stream bed is spatially heterogeneous. Our objective is to introduce a minimum level of additional complexity so as to better match the rupture propagation speed and directionality, at the same time improving the fit between the modeled and observed GPS time series.

Our heterogeneous bed model includes a rate-strengthening region in the middle of the ice stream (Figure 4c). We continue to define $W = 120$ km as the ice stream width, a region which now includes both rate-strengthening and rate-weakening regions. Within the rate-strengthening region we take $(a - b)_{rs} = 0.0075$. Throughout all simulations and over all parts of the ice stream we hold the direct effect parameter $a = 0.02$ fixed. We define W_c as before; that is, we calculate W_c using the properties of the rate-weakening region exclusively. Thus, we anticipate that the critical W/W_c delimiting steady, slow-slip, and fast-slip sliding styles will be somewhat different than in the homogeneous bed case, as will be recurrence periods.

The presence of a central rate-strengthening region gives rise to an even richer variety of rupture propagation styles than before. As described in section 2, ruptures on the WIP are dominantly unilateral from south to

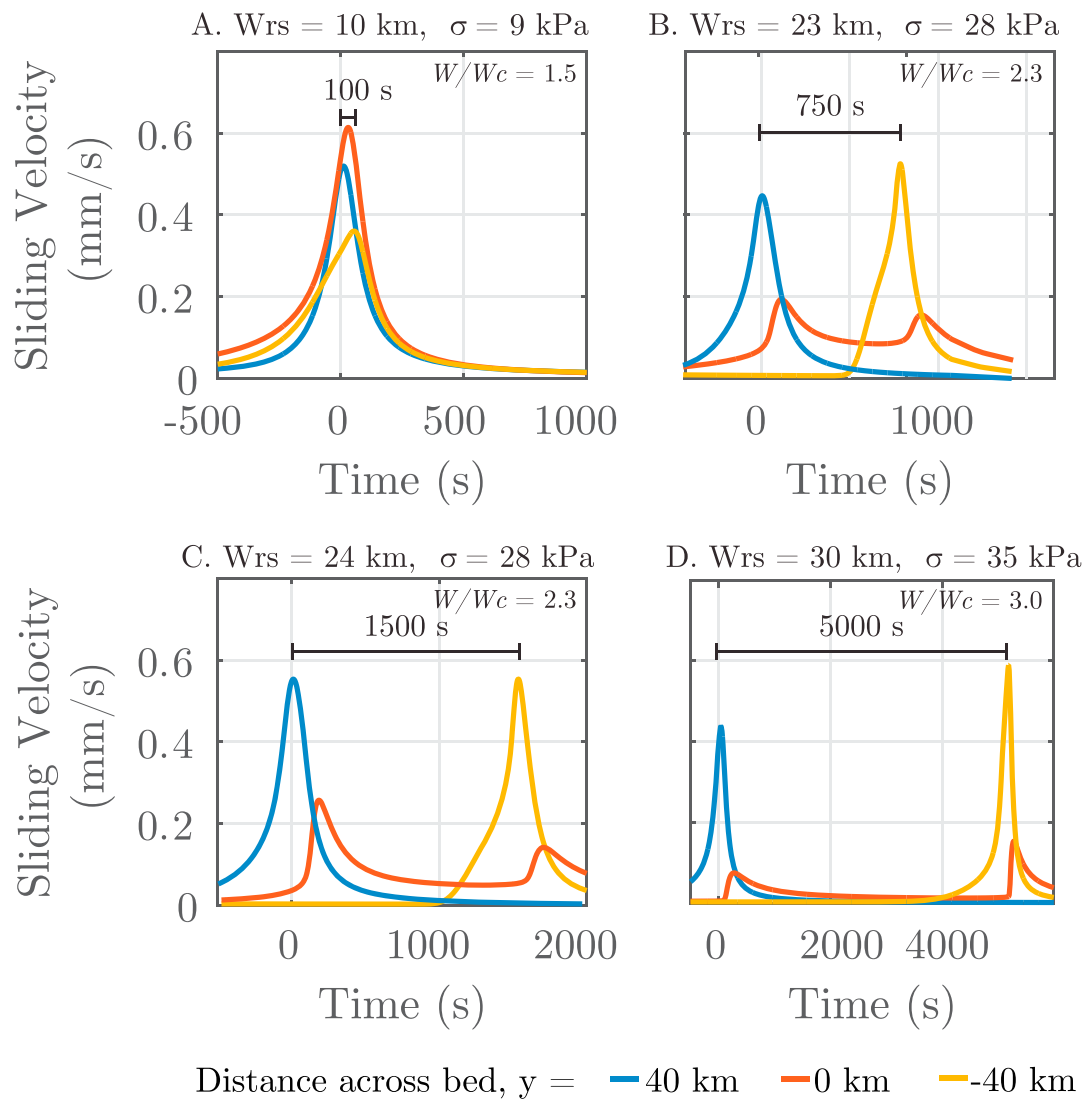


Figure 11. Rupture time across the WIP is governed by the width of a central rate-strengthening region W_{rs} . Each slip event is tuned to the slow-slip regime by changing the effective pressure $\bar{\sigma}$ while holding $d_c = 10$ mm. The simulation in Figure 11b is compared to data in Figure 13.

north. In order to force unilateral ruptures, we make the south (right) rate-weakening region $\approx 1\%$ larger than the north one. Simulations with this geometry often, but not always, result in ruptures that exclusively propagate from south to north. We sometimes, however, observe simulations where ruptures only partially cross the ice stream, leaving behind a stress concentration that makes the subsequent larger. Even for these more complex simulations we still find that ruptures do dominantly tend to favor south to north propagation but may also propagate in the opposite direction or even bilaterally.

We conduct a parameter space study over values of the central rate-strengthening patch width W_{rs} (Figure 11). Given our experience from the previous parts of this paper, we limit attention to the parameters that result in two slow-slip events per day, by tuning d_c and $\bar{\sigma}$ to control the timing and stability of slip events. Two slow-slip events per day occur when $\bar{\sigma}$ is tuned to neutral stability and $d_c = 10$ mm. Figure 11 shows simulations with a heterogeneous bed that fit this description; the tuned value of $\bar{\sigma}$ is given in each plot. We note that the heterogeneous simulations use a smaller d_c compared to the value used for a homogeneous bed (14 mm) due to the stabilizing effect of the rate-strengthening region.

When the central rate-strengthening region is a relatively small (10 km; Figure 11a), slip events are only slightly asymmetric. All points along the ice stream slide in near unison, and because of this there is no clear sense of rupture propagation. Rupture propagation could be induced by increasing W/W_c by decreasing d_c

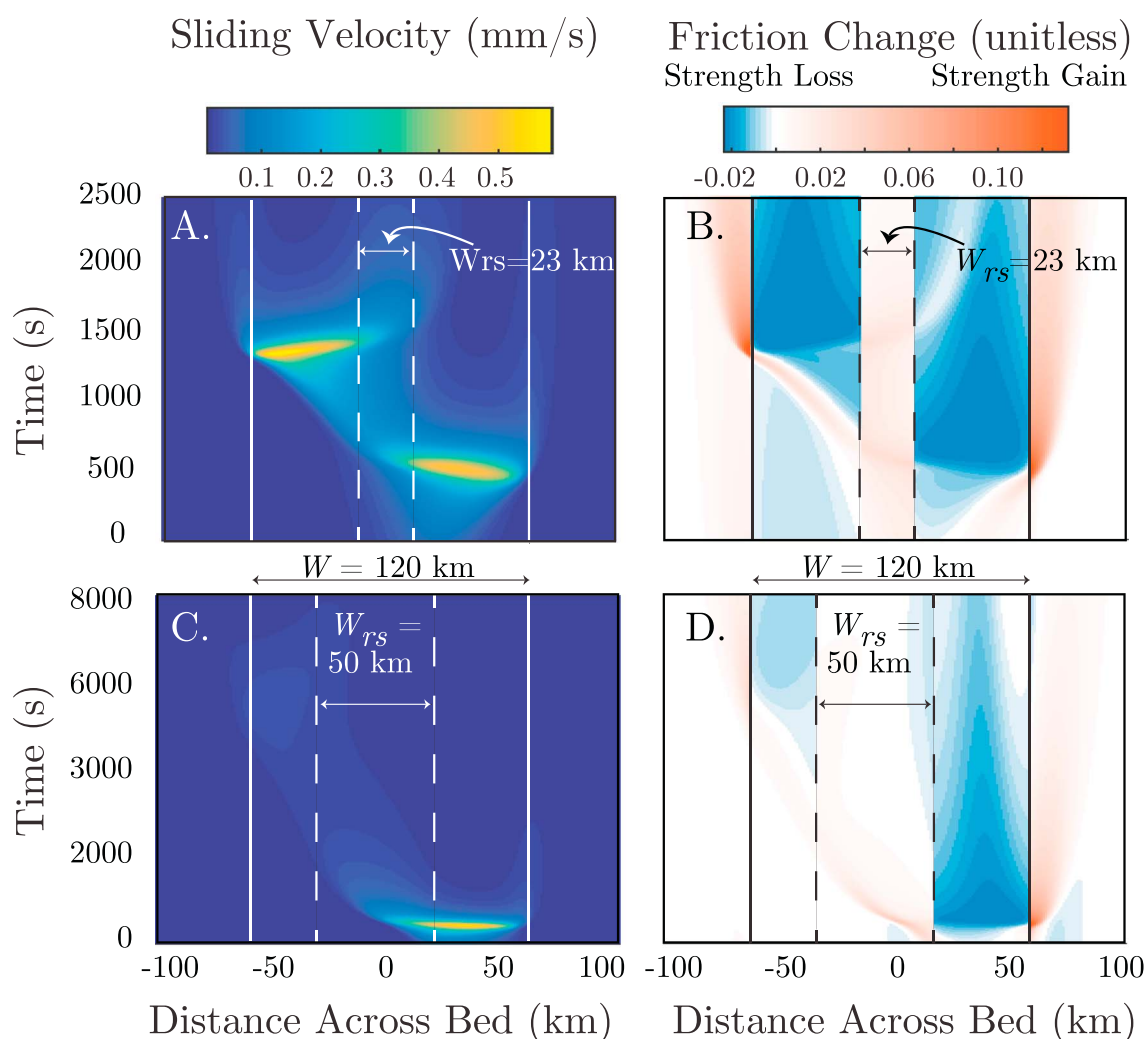


Figure 12. Sliding velocity and basal shear stress perturbation $\tau - f_0 \bar{\sigma}$ from two simulations. (a and b) A simulation with $W_{rs} = 23$ km and $\bar{\sigma} = 28$ kPa that reproduces the WIP slip event timing. (c and d) A simulation with $W_{rs} = 50$ km and $\bar{\sigma} = 50$ kPa, for which the larger central rate-strengthening patch arrests the rupture and prevents it from crossing the ice stream. Vertical solid lines show the ice stream boundary, and vertical dashed lines show the boundary of the rate-strengthening region. The simulation in Figures 12a and 12b is compared to data in Figure 13.

or increasing $\bar{\sigma}$, but this would move the system from the slow-slip to fast-slip regime and would therefore not be consistent with observations from the WIP. Instead, in order to match observations, we must change the size of the central rate-strengthening patch W_{rs} . In Appendix B3 we further quantify when a rate-strengthening region may be considered to be large or small.

For wider rate-strengthening region widths W_{rs} , ruptures tend to propagate from the larger rate-weakening region (blue line Figure 11c) to the smaller rate-weakening region (yellow line in Figure 11c). This sense of rupture propagation begins to emerge when the rate-strengthening region is big enough to experience a significant stress increase. Figure 12 shows space-time plots of the sliding velocity and the basal shear strength changes during this type of slip event. First, rupture nucleates on the right rate-weakening region, causing accelerated slip locally. When the rupture encounters the central rate-strengthening region, a stress increase accompanies the elevation in sliding velocity. Rupture is delayed, but not arrested, by the rate-strengthening region. The rupture reaches the left rate-weakening region, and the stress increase there is sufficiently large to trigger nucleation and subsequent stress drop there. We may therefore exploit this sequence of events to tune the rupture duration and average propagation velocity by changing the size of the rate-strengthening region W_{rs} .

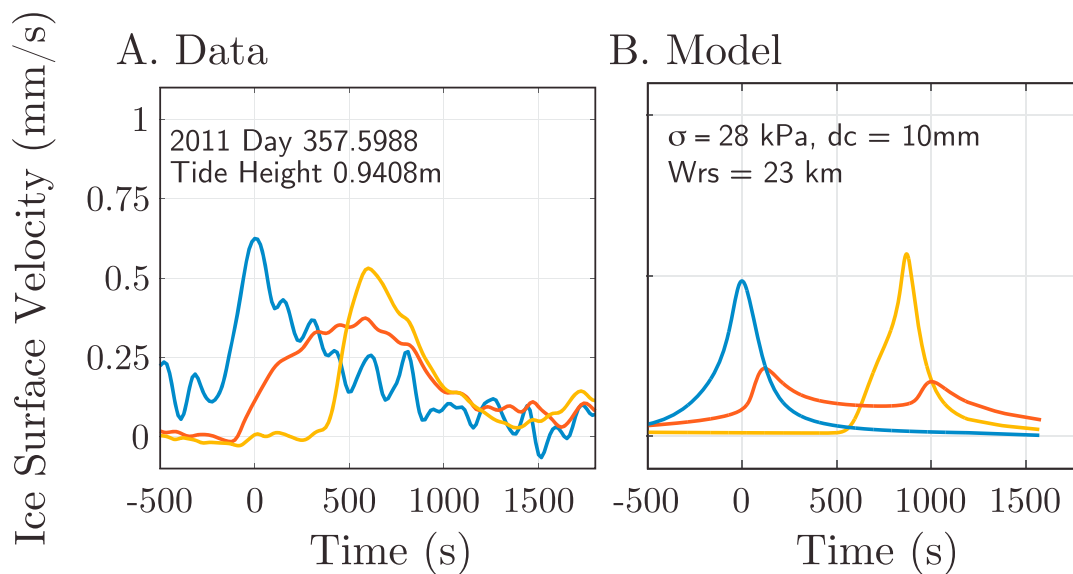


Figure 13. (a) A high tide slip event compared to (b) our preferred model, as discussed in section 7. The slip event (same as in Figure 3g) shows the prominent features of WIP slip events: peak sliding velocity ~ 0.75 mm/s, duration of sliding ~ 1000 s, and a rupture front that travels 80 km in ~ 500 s.

The presence of the rate-strengthening patch alters both slip event recurrence times and maximum sliding velocities. The addition of the rate-strengthening region is a stabilizing effect in the sense that it moves an unstable ice stream dynamical system closer to neutral stability. We described in section 5 how, for a homogeneous ice stream at neutral stability, recurrence periods are shorter and sliding velocities are lower than for a more strongly unstable configuration. This behavior also occurs when the heterogeneous system moves closer to neutral stability. For this reason, both the recurrence period and peak sliding velocities are a decreasing function of rate-strengthening patch size W_{rs} .

Simulations within our preferred range of parameters ($\bar{\sigma} \approx 28$ kPa, $d_c \approx 10$ mm, and $W_{rs} \approx 23$ km) are shown in Figure 13b and are compared against observations in Figure 13a. These parameters result in two slip events per day. Although slip event recurrence times and sliding velocities are not perfectly periodic, as in the homogeneous bed case, the slip events occur during periods of falling tide and the average slip per event is about 50 cm.

In conclusion, we are able to match the observed rupture propagation style of the WIP slip events using an ice stream model with heterogeneous basal friction (Figure 13). There are some differences between the sliding behavior that results from our preferred parameter range and the observations from the WIP (see Figure 13), but the general consistency is perhaps the most that can be expected from a model that resolves only a single horizontal dimension and employs a simplified parameterization of loading. We have shown, however, that heterogeneous basal friction provides an explanation for the observed slow average rupture velocity and unilateral propagation.

8. Discussion

We have presented a cross-stream, antiplane shear, ice stream model that uses rate-and-state friction as a sliding law. This model successfully reproduces the tidally modulated stick-slip cycles at the WIP with the slow-slip style of sliding events. By additionally including a rate-strengthening region in the center of the ice stream, we are able to induce unilateral rupture propagation, as observed on the WIP. By tuning several model parameters to match these observations, we are able to estimate present conditions on the WIP.

8.1. Present Conditions on the WIP

We estimate that the WIP has effective pressure $\bar{\sigma} \approx 28$ kPa and frictional state evolution distance $d_c \approx 10$ mm. Our model best fits the data when the WIP has two rate-weakening regions that are each approximately 48 km wide and are separated by a central rate-strengthening region with width $W_{rs} \approx 23$ km (Figure 4c). Furthermore, this central rate-strengthening region is estimated to have a frictional parameter $(a - b)_{rs} \approx 0.0075$.

Our estimate of basal effective pressure $\bar{\sigma} \approx 28$ kPa is consistent with hydraulic head measurements from boreholes that access the ice-bed interface. Such measurements generally constrain subglacial effective pressures to lie in the range from -10 kPa to $+100$ kPa [Kamb, 2001; Tulaczyk *et al.*, 2014].

We estimate that the bed shear strength at the WIP is $f_0\bar{\sigma} \approx 11$ kPa. Kamb [2001] used a borehole torvane instrument to directly measure bed strength ~ 2 kPa at the UpB camp, several hundred kilometers upstream from the WIP. Joughin *et al.* [2004] inverted ice surface velocity measurements to infer bed shear stresses on the WIP and found values 1.3 – 2.8 kPa, with this range reflecting uncertainty in the model parameterization. However, the study by Joughin *et al.* [2004] as well as other remote sensing studies [Beem *et al.*, 2014; Sergienko *et al.*, 2014] have also found that bed shear stress on the WIP is heterogeneous, with ~ 10 km regions of elevated basal strength as high as ~ 30 – 50 kPa [see, e.g., Joughin *et al.*, 2004, Figure 12]. Because of this heterogeneity, as well as the large distance between the WIP and the UpB site, we consider our estimate of basal shear strength to be consistent with these previous studies.

Lipovsky and Dunham [2016] used seismic tremor that occurs during WIP slip events to estimate subglacial conditions in the vicinity of ~ 1 m seismogenic patches at the ice-bed interface. The most notable difference between their work and the present study is their estimate of the state evolution distance as ~ 1 μm , compared to our value of ~ 10 mm. This 4 orders of magnitude difference is possibly due to a type of frictional upscaling effect. This upscaling hypothesis proposes that the region of the bed that we model as rate-weakening with large d_c might, in reality, be mostly rate-strengthening with a polka-dotted pattern of small rate-weakening patches with small d_c . The upscaling hypothesis is consistent with the observation of seismic tremor in the nucleation region of WIP slip events, because the tremor is explained as the failure of the small rate-weakening regions. Latour *et al.* [2011] demonstrated that the ensemble behavior of such an interface is only sensitive to an appropriately defined average response over the many small tremor regions. Simulations that resolve individual tremor regions with ~ 1 m radius would be required to test this hypothesis.

Our preferred model predicts that there is a third hidden slow-slip event that attempts to nucleate but is sequestered by an unfavorable stressing rate during the rising tide. This hidden slip event is evident in Figure 2b. This event occurs because, under our preferred parameter range, four slip events occur per day when tidal forcing is absent. This finding contradicts the prediction from previous studies that two slip events per day occur in the unforced system [Bindschadler *et al.*, 2003].

We match the observed style of rupture propagation using a rate-strengthening region located between two rate-weakening regions. This characterization is unique among previous studies of WIP slow slip. Previous studies have referred to our rate-weakening regions as sticky spots [Winberry *et al.*, 2011]. We have avoided using the term sticky spot because of the ambiguity surrounding whether this term refers to a region of the bed that is strong (i.e., with anomalously high shear strength; Alley [1993]; Gudmundsson [2003]) versus a region of the bed that experiences stick-slip (i.e., rate-weakening; Anandakrishnan and Alley [1994]; Winberry *et al.* [2011]), these two definitions not being mutually exclusive.

8.2. Past and Future Conditions on the WIP and Other Ice Streams

It is not clear a priori whether the observed deceleration in the WIP stick-slip region is due to glaciological changes local to this region or due to changes in the upstream ice [see, e.g., Beem *et al.*, 2014, Figure 6a]. One line of thinking argues that hydrological changes local to the WIP are resulting in higher effective pressure and therefore stagnation [Retzlaff and Bentley, 1993; Alley *et al.*, 1994; Anandakrishnan and Alley, 1997]. Our model predicts that, if this is indeed the case, then slip events should experience longer recurrence periods and higher slip rates during slip events (e.g., Figure 5). If, on the other hand, the WIP is passively responding to diminished a loading velocity v_0 , then we would expect events to simply have a greater recurrence period but not greater slip rates.

Observations appear to be more consistent with local changes in effective pressure. In particular, Winberry *et al.* [2014a] observed that WIP slip events have been transitioning to longer recurrence periods and higher sliding rates. We tentatively note that this is consistent with our model predictions but caution that inclusion of ice viscosity and subglacial hydrology into our model, as will be discussed subsequently, may somewhat alter this finding.

If past subglacial conditions had higher basal pore water pressures, our model predicts that WIP sliding was tidally modulated but without stick-slip cycles at this time (Figure 7). It might be possible to test this hypothesis using historical seismograms, provided that such records would be sensitive enough to conclusively detect

slip events, if they were occurring in the past. Similarly, our model predicts that the Kamb Ice Stream may have had stick-slip events during its stagnation and also that other ice streams will experience stick-slip if other ice streams stagnate due to declining pore water pressure.

8.3. Possible Extensions of Our Model

Despite matching many features of the WIP events, there remain several open questions and there are obvious extensions to the model that would make it more realistic. Here we briefly discuss these.

Perhaps the most unsettling aspect of our idealized model of the WIP is the narrow range of parameter space in which the model matches the observations. The model is quite sensitive in the sense that small perturbations to our preferred parameter set result in rather different sliding behaviors. Small perturbations in the basal water pressure, for example, may trigger the transition from slow-slip events to fast-slip ruptures propagating close to the shear wave speed. While we cannot rule out the possibility that the WIP could transition to this sliding style, the lack of observational evidence for that sliding style in other glaciers and ice streams, as well as the possibility that stagnation may occur for large effective pressures, makes it seem unlikely. For this reason, it is certainly worth examining additional slip-stabilizing processes. Dilatant strengthening of till and fault gouge has been suggested to stabilize sliding [Clarke, 1987; Moore and Iverson, 2002; Segall et al., 2010]. Another possibility is that the rate dependency of friction ($a - b$) changes from rate-weakening to rate-strengthening as sliding velocity increases above some threshold. Such behavior has been proposed in the context of subduction zone slow-slip events [Shibazaki and Iio, 2003; Shibazaki and Shimamoto, 2007] and has been observed in some friction experiments [e.g., Shimamoto, 1986; Kilgore et al., 1993]. A related hypothesis, first suggested by Zoet et al. [2013] and recently elaborated upon by McCarthy et al. [2017], is that the ice-bed interface may transition to rate-strengthening behavior due to thermal effects associated with elevated slip rates.

Even more broadly speaking, a fundamental question arising out of our work is what physical processes are responsible for rate-strengthening and rate-weakening behavior? We have adopted rate-and-state friction as a sliding law, viewing it as a convenient mathematical framework in which to introduce rate dependence of friction that could arise from a host of processes. The advantage of the empirical nature of rate-and-state friction is that its parameters can be extracted from friction experiments. As described in section 1, there have been many experimental studies on glacial materials [Tulaczyk et al., 2000; Thomason and Iverson, 2008; Rathbun et al., 2008; Iverson, 2010; Schulson and Fortt, 2012; Zoet et al., 2013; Zoet and Iverson, 2015; McCarthy et al., 2016; Zoet and Iverson, 2016; McCarthy et al., 2017]. We are not aware, however, of any experimental study to do either velocity-stepping or slide-hold-slide experiments on glacial till collected from beneath an active ice stream. Experiments done with realistic pore pressure conditions, and with wide grain size distributions, provide additional value [Thomason and Iverson, 2008]. In general, more experiments that quantify the strength of subglacial materials, especially under unsteady loading conditions, would constitute a major contribution to the field.

The evolution of the subglacial hydrological system is likely to affect ice dynamics at the decadal timescale relevant to the slowdown of the WIP [Suckale et al., 2014; Rosier et al., 2015; Thompson et al., 2014]. Lipovsky and Dunham [2016] noted that the ice-bed interface became more stiff during long recurrence periods between slip events at the WIP. Recent laboratory studies have followed up on this observation and noted that such a stiffness change may occur due to till dewatering [Leeman et al., 2016]. Till dewatering is likely caused by cyclic loading rather than melt-thaw cycles [Iverson, 2010] as previously proposed [Winberry et al., 2009; Walter et al., 2011]. Together, these results generally appear to be consistent with the idea that tidal stress variations induce effective pressure variations that lead to variations in till strength and elastic properties [Sayag and Worster, 2011, 2013; Walker et al., 2013; Luthra et al., 2016]. Our neglect of these processes prevents us from analyzing many interesting patterns in the WIP slip events including correlations between tides and rupture velocities [Walter et al., 2015] and correlations between subglacial lake activity and slip event timing [Siegfried et al., 2016]. To capture these processes, we would need to extend our model with a coupled description of subglacial hydrology. With regard to modeling longer time periods, it will also be essential to account for ice viscosity [Winberry et al., 2014a; Goldberg et al., 2014].

The finding that WIP slip events are in the slow-slip limit has important implications for the representation of basal sliding in numerical ice sheet models. Because it is not clear a priori whether inertia plays a role in the WIP slip events, we have retained these effects for this study. However, because of the finding that slip events are in the slow-slip limit, future studies may wish to neglect the effects of elastic waves. Such a quasi-static, non-inertial model was used, for example, by Goldberg et al. [2014]. Future models could additionally be improved

in a geometrical sense by switching to a fully two-dimensional (thickness-averaged map view) representation that would permit a more rigorous description of the ice bordering the ice stream (i.e., floating versus grounded) and the loading from inflowing ice.

8.4. Conclusions

We use rate-and-state friction as an ice sheet sliding law. Although other sliding laws may be able to fit some aspects of the observations, in this study we have attempted to closely follow the laboratory-derived constitutive behavior of glacial materials. Furthermore, our study provides a type of empirical validation of rate-and-state friction as a glacier sliding law. As such, this work paves the way to a more realistic description of the evolving strength of the ice-bed interface.

Appendix A: Examination of Bed Elastic Motions

In this appendix we justify the approximation of negligible elastic deformation of the ice stream bed. To analyze this case, we consider the depth-resolved streamwise momentum balance (compare, for example, the depth-averaged momentum balance of equation (1)),

$$\rho \frac{\partial^2 u'}{\partial t^2} = G \left(\frac{\partial^2 u'}{\partial y^2} + \frac{\partial^2 u'}{\partial z^2} \right). \quad (\text{A1})$$

We have introduced the notation $u'(y, z)$ to denote the depth-resolved ice displacement in the x direction. We have neglected the loading terms as they do not affect our analysis, which follows previous work on sliding between elastic materials [Geubelle and Rice, 1995; Ranjith and Rice, 2001; Ranjith, 2014].

We transform (A1) using the transform of an arbitrary function $f(y, z, t)$

$$\hat{f}(k, z, \omega) = \int_{-\infty}^{\infty} \int_{-\infty}^{\infty} f(y, z, t) e^{-i(ky - \omega t)} dt dy. \quad (\text{A2})$$

With this transform, the general solution of equation (A1) is

$$\hat{u} = c_1 \exp(-|k|\alpha z) + c_2 \exp(|k|\alpha z), \quad (\text{A3})$$

for constants c_1 and c_2 and

$$\alpha^2 = 1 - \left(\frac{\omega}{kc} \right)^2, \quad (\text{A4})$$

where $c = \sqrt{G/\rho}$ is the shear wave speed.

Our goal is to derive a relationship between the elastic bed shear stress and slip. We denote the elastic bed shear stress

$$\tau = G \left. \frac{\partial u}{\partial z} \right|_{z=0}. \quad (\text{A5})$$

We then evaluate the stress and slip along the bed. We use the notation that the transform of τ is \hat{T} and the transform of $\hat{u}'(k, z = 0, t)$ is $\hat{U}(k, \omega)$.

We next enforce the interface conditions. Although equations (A1), (A3), and (A4) were written to describe the displacement field in the ice, identical equations describe the motion of the bed. We therefore introduce subscripts i and b to denote material fields of the ice and bed. Continuity of tractions across the bed require that

$$\hat{T}_i = \hat{T}_b. \quad (\text{A6})$$

We define the transform of slip as

$$\hat{D} = \hat{U}_i - \hat{U}_b. \quad (\text{A7})$$

We take $z = H$ to be a traction-free surface and assume that displacements vanish as $y \rightarrow -\infty$.

The relationship between \hat{D} and \hat{T} is then given by

$$\hat{D}(k, \omega) = |k|^{-1} \left[\frac{1}{\alpha_b G_b} + \frac{1}{\alpha_i G_i \tanh(\alpha_i H |k|)} \right] \hat{T}(k, \omega). \quad (\text{A8})$$

The two terms in the brackets in equation (A8) have the interpretation of the bed and ice elastic compliances. In the thin-layer limit, $\tanh(\alpha_i H|k|) \approx \alpha_i H|k|$. The relative importance of bed and ice elastic deformation is then given by the compliance ratio

$$\frac{H|k|G_i}{G_b} \sim \frac{H}{W} \frac{G_i}{G_b}. \quad (\text{A9})$$

Here we have assumed that elastic deformation is quasi-static ($\alpha_b \approx \alpha_i \approx 1$), consistent with our main focus on slow-slip events. In the scaling relation of equation (A9) we have assumed that wavelengths of interest are on the order of the ice stream width W ; the argument becomes even stronger when considering shorter wavelengths. Using $H = 1$ km, $W = 100$ km, and $G_i/G_b = 0.1$ gives the relative importance of ice elastic motion to bed elastic motion to be on the order of 10^3 . For this reason, we neglect bed elastic motion in our analysis.

Appendix B: Linearized Stability Analysis

In this appendix we linearize the governing equations to study the stability of small perturbations about steady sliding. Although we focus on the linearized system, recent work [Viesca, 2016b] has described the nonlinear dynamics of this system as well.

B1. Linearized Governing Equations

We linearize the basal shear stress relation of equation (12) about steady sliding at velocity v_0 and shear stress

$$\tau_0 = \bar{\sigma} f_{ss}(v_0). \quad (\text{B1})$$

We add small perturbations of the form $v = v_0 + \delta v$ and $\tau = \tau_0 + \delta \tau$. The Laplace-transformed friction law (equations (12) and (13)) is

$$\delta \tau = \frac{a\sigma}{s + v_0/d_c} \left(s - \frac{v_0}{d_c} \frac{b-a}{a} \right) \frac{\delta v}{v_0}, \quad (\text{B2})$$

where s is the Laplace transform variable. In writing this we have eliminated the state variable.

We then substitute this expression for shear stress τ (equation (B2)) into the momentum balance equation (7), which is already a linear equation. We take the spatial Fourier transform with wave number k . The result is

$$A(k, s) \equiv \frac{GH}{s/v_0} \left(k^2 + \frac{s^2}{c^2} + \frac{G^*/G}{L^2} \right) + \bar{\sigma} \left(as - \frac{b-a}{d_c/v_0} \right) \left(s + \frac{v_0}{d_c} \right)^{-1} = 0. \quad (\text{B3})$$

This is the same characteristic equation found by Ranjith [2014, equation 44] in the limit that the material beneath the layer is infinitely rigid.

Equation (B3) is a cubic equation in the Laplace transform variable s . As such, equation (B3) always has three solutions or roots. For a particular set of parameters, these three roots are plotted in Figure B1 for the case of rate-weakening friction and in Figure B2 for the case of rate-strengthening friction. One root is always purely real and negative. The other two roots are either purely real or, when complex, come as a complex conjugate pair.

B2. Neutral Stability and the Influence of Inertia

Consider rate-weakening friction ($b - a > 0$). The most important analytical result concerns the transition from stable to unstable sliding, which occurs as the wave number is decreased below a critical wave number. At this point, the real part of a complex conjugate pair of roots changes sign (with nonzero imaginary part). This occurs when the wave number $k \equiv 2\pi/\lambda$ is equal to its critical value,

$$k_c \equiv \sqrt{\frac{\bar{\sigma}(b-a)}{HGd_c} - \frac{\bar{\sigma}(b-a)}{G_*L^2} \sqrt{1+q^2}}, \quad (\text{B4})$$

where

$$q \equiv v_0 / \sqrt{\frac{a\bar{\sigma}d_c}{\rho H}}. \quad (\text{B5})$$

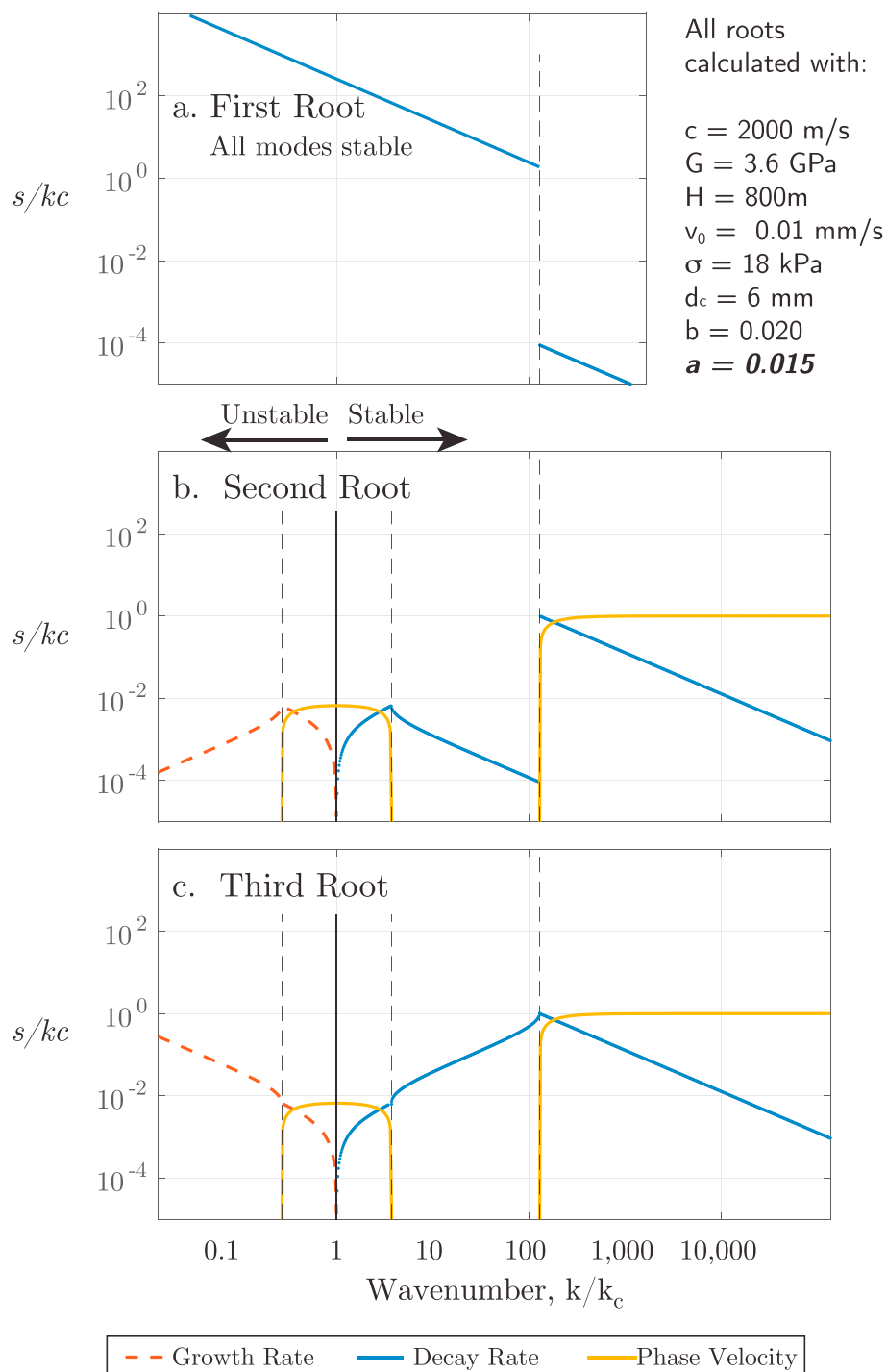


Figure B1. Roots of the linearized governing equations. The instability that gives rise to stick-slip cycles occurs when $k/k_c < 1$ in the (b) second and (c) third roots. Roots are calculated neglecting streamwise stiffness. (a) A mode that is unconditionally stable and therefore never has a defined growth rate (i.e., no red dashed line).

The parameter q quantifies the influence of inertial effects on the critical wave number k_c . It is of interest that the inertial parameter q does not involve the elastic properties of the system and instead only depends on the inertial properties, i.e., the density. For the parameters used that are able to match the properties of the WIP slip events, $q \ll 1$ and inertial effects are unimportant for the purposes of determining the stability of sliding.

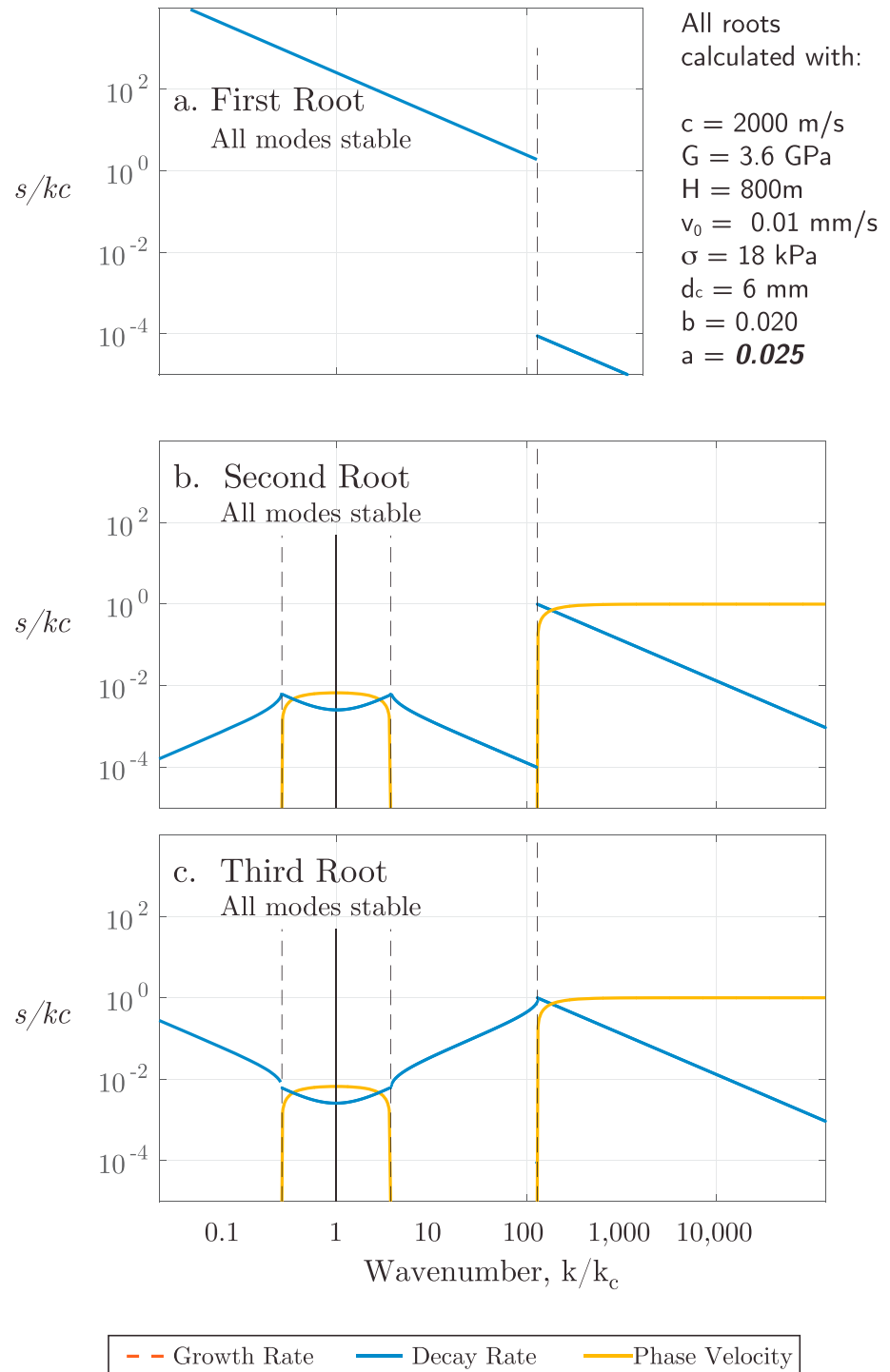


Figure B2. Same as Figure B1, except for a rate-strengthening material. In this case there is no stick-slip instability and the roots of the dispersion relation always have nonpositive real part. Roots are calculated neglecting streamwise stiffness.

The frequency of the neutrally stable mode ω_c is identical to that in the whole-space case studied by Rice *et al.* [2001],

$$\text{Im } s|_{\text{Re } s=0} \equiv \omega_c = \sqrt{\frac{b-a}{a}} \frac{v_0}{d_c}. \quad (\text{B6})$$

This frequency is independent of the inertial and elastic properties of ice. From this frequency we define

$$T_c \equiv \frac{2\pi}{\omega_c}. \quad (\text{B7})$$

B3. The Rate-Strengthening Response

When $a - b > 0$, the frictional response is rate-strengthening (Figure B2) and solutions to equation (B3) are unconditionally stable. Although there is no range of wave numbers over which perturbations grow in time, the decay rate has a local minima at a wave number k_s defined by

$$k_s \equiv \sqrt{\frac{\sigma(a-b)}{HGd_c} - \frac{\sigma(a-b)}{G_*L^2} \sqrt{1+q^2}}, \quad (\text{B8})$$

where q is defined as in equation (B5).

Appendix C: Numerical Aspects of WIP Stick-Slip

We use a modified form of the frictional state evolution equation (13) in our numerical implementation. This form has the numerical benefit of avoiding logarithms. We make the substitution

$$\psi \equiv b \log \left(\frac{v_0 \theta}{d_c} \right). \quad (\text{C1})$$

The state evolution equation in terms of this new state variable is

$$\dot{\psi} = \frac{v_0}{d_c} \left[\exp \frac{f_0 - \psi}{b} - \frac{v}{v_0} \right]. \quad (\text{C2})$$

The equations are solved numerically in first-order form using the state variable ψ , sliding velocity v , and displacement u as the dependent variables. We make all calculated quantities order unity and so implement stresses in kilopascals, displacement in millimeters, distance in kilometers, elastic moduli in gigapascals, and wave speeds in kilometers per second.

Time stepping is done using the MATLAB Runge-Kutta solver for stiff equations, *ode15s*. This is an implicit, variable-step, variable-order solver that uses numerical differentiation formulas. All simulations discussed in this work are run for a sufficient period such that steady limit cycles form.

The spatial domain is discretized using N points, and the second spatial derivative operator is discretized using a fourth-order-accurate finite difference stencil. We vary N so that W_c is always resolved with ~ 100 points. This typically leads to N in the range of 400–1200. Boundary conditions are weakly enforced [Mattsson and Nordström, 2004; Mattsson *et al.*, 2009]. The spatial difference operator transitions to one-sided derivatives near the boundary in a manner that is provably stable using a summation-by-parts construction.

Acknowledgments

Daniel Goldberg, Bryn Hubbard, and an anonymous reviewer contributed feedback that improved the quality of this manuscript. J. Paul Winberry assisted us with the GPS data. This manuscript benefited from several discussions with Rob Viesca, Matt Siegfried, Slawek Tulaczyk, Susan Schwartz, and Grace Barcheck. This work was supported by the National Science Foundation (PLR-1542885). All of the data used in this study were previously published and are available through DOI:10.7283/T5SQ8XPC.

References

- Adalgeirsdóttir, G., A. M. Smith, T. Murray, M. King, K. Makinson, K. W. Nicholls, and A. Behar (2008), Tidal influence on Rutford Ice Stream, West Antarctica: Observations of surface flow and basal processes from closely spaced GPS and passive seismic stations, *J. Glaciol.*, *54*(187), 715–724, doi:10.3189/002214308786570872.
- Ader, T. J., N. Lapusta, J.-P. Avouac, and J.-P. Ampuero (2014), Response of rate-and-state seismogenic faults to harmonic shear-stress perturbations, *Geophys. J. Int.*, *198*(1), 385–413, doi:10.1093/gji/ggu144.
- Alley, R. (1993), In search of ice-stream sticky spots, *J. Glaciol.*, *39*(133), 447–454.
- Alley, R., S. Anandakrishnan, C. Bentley, and N. Lord (1994), A water-piracy hypothesis for the stagnation of Ice Stream C, Antarctica, *Ann. Glaciol.*, *20*(1), 187–194, doi:10.1029/96GL04016.
- Ampuero, J.-P., and A. M. Rubin (2008), Earthquake nucleation on rate and state faults—Aging and slip laws, *J. Geophys. Res.*, *113*, B01302, doi:10.1029/2007JB005082.
- Anandakrishnan, S., and R. Alley (1994), Ice Stream C, Antarctica, sticky spots detected by microearthquake monitoring, *Ann. Glaciol.*, *20*(1), 183–186.
- Anandakrishnan, S., and R. B. Alley (1997), Stagnation of Ice Stream C, West Antarctica by water piracy, *Geophys. Res. Lett.*, *24*(3), 265–268.

- Anandakrishnan, S., and C. Bentley (1993), Micro-earthquakes beneath Ice Streams B and C, West Antarctica: Observations and implications, *J. Glaciol.*, *39*, 455–462.
- Anandakrishnan, S., D. Voigt, R. Alley, and M. King (2003), Ice Stream D flow speed is strongly modulated by the tide beneath the Ross Ice Shelf, *Geophys. Res. Lett.*, *30*(7), 1361, doi:10.1029/2002GL016329.
- Balanov, A., N. Janson, D. Postnov, and O. Sosnovtseva (2009), *Synchronization: From Simple to Complex*, Springer Ser. in Synergetics, Springer, Berlin.
- Beeler, N., and D. Lockner (2003), Why earthquakes correlate weakly with the solid earth tides: Effects of periodic stress on the rate and probability of earthquake occurrence, *J. Geophys. Res.*, *108*(B8), 2391, doi:10.1029/2001JB001518.
- Beem, L., S. Tulaczyk, M. King, M. Bougamont, H. Fricker, and P. Christoffersen (2014), Variable deceleration of Whillans Ice Stream, West Antarctica, *J. Geophys. Res. Earth Surf.*, *119*, 212–224, doi:10.1002/2013JF002958.
- Bindschadler, R. A., M. A. King, R. B. Alley, S. Anandakrishnan, and L. Padman (1987), Till beneath Ice Stream B: 1. Properties derived from seismic travel times, *J. Geophys. Res.*, *92*(B9), 8903–8911.
- Bindschadler, R. A., M. A. King, R. B. Alley, S. Anandakrishnan, and L. Padman (2003), Tidally controlled stick-slip discharge of a West Antarctic ice stream, *Science*, *301*(5636), 1087–1089, doi:10.1126/science.1087231.
- Bougamont, M., S. Price, P. Christoffersen, and A. Payne (2011), Dynamic patterns of ice stream flow in a 3-D higher-order ice sheet model with plastic bed and simplified hydrology, *J. Geophys. Res.*, *116*, F04018, doi:10.1029/2011JF002025.
- Bougamont, M., P. Christoffersen, S. F. Price, H. A. Fricker, S. Tulaczyk, and S. P. Carter (2015), Reactivation of Kamb Ice Stream tributaries triggers century-scale reorganization of Siple Coast ice flow in West Antarctica, *Geophys. Res. Lett.*, *42*, 8471–8480, doi:10.1002/2015GL065782.
- Byerlee, J. D. (1967), Frictional characteristics of granite under high confining pressure, *J. Geophys. Res.*, *72*, 3639–3648.
- Clarke, G. K. (1987), Subglacial till: A physical framework for its properties and processes, *J. Geophys. Res.*, *92*(B9), 9023–9036.
- Cuffey, K. M., and W. S. B. Paterson (2010), *The Physics of Glaciers*, Academic Press, New York.
- Danesi, S., S. Bannister, and A. Morelli (2007), Repeating earthquakes from rupture of an asperity under an Antarctic outlet glacier, *Earth Planet. Sci. Lett.*, *253*(1), 151–158, doi:10.1016/j.epsl.2006.10.023.
- Dieterich, J. (2007), Applications of rate- and state-dependent friction to models of fault slip and earthquake occurrence, *Treatise Geophys.*, *4*, 107–129, doi:10.1016/B978-0-444-52748-6/00065-1.
- Dieterich, J. H. (1972), Time-dependent friction in rocks, *J. Geophys. Res.*, *77*(20), 3690–3697.
- Dieterich, J. H. (1979), Modeling of rock friction: 1. Experimental results and constitutive equations, *J. Geophys. Res.*, *84*(B5), 2161–2168.
- Dieterich, J. H., and B. D. Kilgore (1994), Direct observation of frictional contacts: New insights for state-dependent properties, *Pure Appl. Geophys.*, *143*, 283–302.
- Dragert, H., K. Wang, and T. S. James (2001), A silent slip event on the deeper Cascadia subduction interface, *Science*, *292*(5521), 1525–1528.
- Feldmann, J., and A. Levermann (2016), From Heinrich events to cyclic ice streaming: The grow-and-surge instability in the parallel ice sheet model, *Cryosphere Discuss.*, *2016*, 1–19, doi:10.5194/tc-2016-235.
- Fretwell, P., et al. (2013), Bedmap2: Improved ice bed, surface and thickness datasets for Antarctica, *Cryosphere*, *7*(1), 375–393.
- Geubelle, P. H., and J. R. Rice (1995), A spectral method for three-dimensional elastodynamic fracture problems, *J. Mech. Phys. Solids*, *43*(11), 1791–1824.
- Goldberg, D., C. Schoof, and O. Sergienko (2014), Stick-slip motion of an Antarctic ice stream: The effects of viscoelasticity, *J. Geophys. Res. Earth Surf.*, *119*, 1564–1580, doi:10.1002/2014JF003132.
- Gudmundsson, G. H. (2003), Transmission of basal variability to a glacier surface, *J. Geophys. Res.*, *108*(B5), 2253, doi:10.1029/2002JB002107.
- Gudmundsson, G. H. (2006), Fortnightly variations in the flow velocity of Rutford Ice Stream, West Antarctica, *Nature*, *444*(7122), 1063–1064.
- Harig, C., and F. J. Simons (2015), Accelerated West Antarctic ice mass loss continues to outpace East Antarctic gains, *Earth Planet. Sci. Lett.*, *415*, 134–141.
- Heinrich, H. (1988), Origin and consequences of cyclic ice rafting in the northeast Atlantic Ocean during the past 130,000 years, *Quat. Res.*, *29*(2), 142–152.
- Hemming, S. R. (2004), Heinrich events: Massive late Pleistocene detritus layers of the North Atlantic and their global climate imprint, *Rev. Geophys.*, *42*, RG1005, doi:10.1029/2003RG000128.
- Ito, Y., K. Obara, K. Shiomi, S. Sekine, and H. Hirose (2007), Slow earthquakes coincident with episodic tremors and slow slip events, *Science*, *315*(5811), 503–506.
- Iverson, N. R. (2010), Shear resistance and continuity of subglacial till: Hydrology rules, *J. Glaciol.*, *56*(200), 1104–1114, doi:10.3189/002214311796406220.
- Joughin, I., S. Tulaczyk, R. Bindschadler, and S. F. Price (2002), Changes in West Antarctic ice stream velocities: Observation and analysis, *J. Geophys. Res.*, *107*(B11), 2289, doi:10.1029/2001JB001029.
- Joughin, I., D. R. MacAyeal, and S. Tulaczyk (2004), Basal shear stress of the Ross Ice Streams from control method inversions, *J. Geophys. Res.*, *109*, B09405, doi:10.1029/2003JB002960.
- Kamb, B. (2001), Basal zone of the West Antarctic ice streams and its role in lubrication of their rapid motion, in *The West Antarctic Ice Sheet: Behavior and Environment*, vol. 77, edited by R. B. Alley and R. A. Bindschadler, pp. 157–199, AGU, Washington, D. C., doi:10.1029/AR077p0157.
- Kilgore, B. D., M. L. Blanpied, and J. H. Dieterich (1993), Velocity dependent friction of granite over a wide range of conditions, *Geophys. Res. Lett.*, *20*(10), 903–906.
- Kyrke-Smith, T., R. Katz, and A. Fowler (2014), Subglacial hydrology and the formation of ice streams, *Proc. R. Soc. A*, *470*(2161), 20130494, doi:10.1098/rspa.2013.0494.
- Latour, S., M. Campillo, C. Voisin, I. Ionescu, J. Schmedes, and D. Lavallée (2011), Effective friction law for small-scale fault heterogeneity in 3D dynamic rupture, *J. Geophys. Res.*, *116*, B10306, doi:10.1029/2010JB008118.
- Leeman, J., R. Valdez, R. Alley, S. Anandakrishnan, and D. Saffer (2016), Mechanical and hydrologic properties of Whillans Ice Stream till: Implications for basal strength and stick-slip failure, *J. Geophys. Res. Earth Surf.*, *120*, 1295–1309, doi:10.1002/2016JF003863.
- Lliboutry, L. (1968), General theory of subglacial cavitation and sliding of temperate glaciers, *J. Glaciol.*, *7*(49), 21–58.
- Lipovsky, B., and E. Dunham (2016), Tremor during ice-stream stick slip, *Cryosphere*, *10*(1), 385–399, doi:10.5194/tc-10-385-2016.
- Liu, Y., and J. R. Rice (2005), Aseismic slip transients emerge spontaneously in three-dimensional rate and state modeling of subduction earthquake sequences, *J. Geophys. Res.*, *110*, B08307, doi:10.1029/2004JB003424.
- Liu, Y., and J. R. Rice (2007), Spontaneous and triggered aseismic deformation transients in a subduction fault model, *J. Geophys. Res.*, *112*, B09404, doi:10.1029/2007JB004930.
- Luthra, T., S. Anandakrishnan, J. P. Winberry, R. B. Alley, and N. Holschuh (2016), Basal characteristics of the main sticky spot on the ice plain of Whillans Ice Stream, Antarctica, *Earth Planet. Sci. Lett.*, *440*, 12–19.

- MacAyeal, D. (1993), Binge/purge oscillations of the Laurentide Ice Sheet as a cause of the North Atlantic's Heinrich events, *Paleoceanography*, 8(6), 775–784.
- Madariaga, R. (1976), Dynamics of an expanding circular fault, *Bull. Seismol. Soc. Am.*, 66, 639–666.
- Marone, C. (1998), Laboratory-derived friction laws and their application to seismic faulting, *Annu. Rev. Earth Planet. Sci.*, 26(1), 643–696.
- Marone, C., C. B. Raleigh, and C. H. Scholz (1990), Frictional behavior and constitutive modeling of a simulated fault gouge, *J. Geophys. Res.*, 95(B5), 7007–7025.
- Marsh, O., W. Rack, D. Floricioiu, N. Golledge, and W. Lawson (2013), Tidally induced velocity variations of the Beardmore Glacier, Antarctica, and their representation in satellite measurements of ice velocity, *Cryosphere*, 7(5), 1375–1384.
- Mattsson, K., and J. Nordström (2004), Summation by parts operators for finite difference approximations of second derivatives, *J. Comput. Phys.*, 199(2), 503–540.
- Mattsson, K., F. Ham, and G. Iaccarino (2009), Stable boundary treatment for the wave equation on second-order form, *J. Sci. Comput.*, 41(3), 366–383.
- McCarthy, C., H. Savage, T. Koczyński, and M. Nielson (2016), An apparatus to measure frictional, anelastic, and viscous behavior in ice at temperate and planetary conditions, *Rev. Sci. Instrum.*, 87(5), 055112.
- McCarthy, C., H. Savage, and M. Nettles (2017), Temperature dependence of ice-on-rock friction at realistic glacier conditions, *Philos. Trans. R. Soc. A*, 375(2086), 20150348.
- Minchew, B., M. Simons, B. Riel, and P. Milillo (2016), Tidally induced variations in vertical and horizontal motion on Rutford Ice Stream, West Antarctica, inferred from remotely sensed observations, *J. Geophys. Res. Earth Surf.*, 122, 167–190, doi:10.1002/2016JF003971.
- Moore, P. L., and N. R. Iverson (2002), Slow episodic shear of granular materials regulated by dilatant strengthening, *Geology*, 30(9), 843–846.
- Nakatani, M. (2001), Conceptual and physical clarification of rate and state friction: Frictional sliding as a thermally activated rheology, *J. Geophys. Res.*, 106(B7), 13,347–13,380.
- Obara, K. (2002), Nonvolcanic deep tremor associated with subduction in southwest Japan, *Science*, 296(5573), 1679–1681.
- Padman, L., H. A. Fricker, R. Coleman, S. Howard, and L. Erofeeva (2002), A new tide model for the Antarctic ice shelves and seas, *Ann. Glaciol.*, 34(1), 247–254.
- Peng, Z., and J. Gomberg (2010), An integrated perspective of the continuum between earthquakes and slow-slip phenomena, *Nat. Geosci.*, 3(9), 599–607.
- Pratt, M. J., J. P. Winberry, D. A. Wiens, S. Anandakrishnan, and R. B. Alley (2014), Seismic and geodetic evidence for grounding-line control of Whillans Ice Stream stick-slip events, *J. Geophys. Res. Earth Surf.*, 119, 333–348, doi:10.1002/2013JF002842.
- Ranjith, K. (2014), Instabilities in dynamic anti-plane sliding of an elastic layer on a dissimilar elastic half-space, *J. Elast.*, 115(1), 47–59, doi:10.1007/s10659-013-9446-1.
- Ranjith, K., and J. R. Rice (2001), Slip dynamics at an interface between dissimilar materials, *J. Mech. Phys. Solids*, 49(2), 341–361.
- Rathbun, A. P., and C. Marone (2010), Effect of strain localization on frictional behavior of sheared granular materials, *J. Geophys. Res.*, 115, B01204, doi:10.1029/2009JB006466.
- Rathbun, A. P., C. Marone, R. B. Alley, and S. Anandakrishnan (2008), Laboratory study of the frictional rheology of sheared till, *J. Geophys. Res.*, 113, F02020, doi:10.1029/2007JF000815.
- Retzlaff, R., and C. R. Bentley (1993), Timing of stagnation of Ice Stream C, West Antarctica, from short-pulse radar studies of buried surface crevasses, *J. Glaciol.*, 39(133), 553–561.
- Rice, J., and A. Ruina (1983), Stability of steady frictional slipping, *J. Appl. Mech.*, 50(2), 343–349.
- Rice, J. R. (1993), Spatio-temporal complexity of slip on a fault, *J. Geophys. Res.*, 98(B6), 9885–9907.
- Rice, J. R. (2006), Heating and weakening of faults during earthquake slip, *J. Geophys. Res.*, 111, B05311, doi:10.1029/2005JB004006.
- Rice, J. R., N. Lapusta, and K. Ranjith (2001), Rate and state dependent friction and the stability of sliding between elastically deformable solids, *J. Mech. Phys. Solids*, 49(9), 1865–1898, doi:10.1016/S0022-5096(01)00042-4.
- Rignot, E., J. L. Bamber, M. R. Van Den Broeke, C. Davis, Y. Li, W. J. Van De Berg, and E. Van Meijgaard (2008), Recent Antarctic ice mass loss from radar interferometry and regional climate modelling, *Nat. Geosci.*, 1(2), 106–110.
- Robel, A. A., E. DeGiuli, C. Schoof, and E. Tziperman (2013), Dynamics of ice stream temporal variability: Modes, scales, and hysteresis, *J. Geophys. Res. Earth Surf.*, 118, 925–936, doi:10.1002/jgrf.20072.
- Rogers, G., and H. Dragert (2003), Episodic tremor and slip on the Cascadia subduction zone: The chatter of silent slip, *Science*, 300(5627), 1942–1943.
- Rosier, S. H. R., and G. H. Gudmundsson (2016), Tidal controls on the flow of ice streams, *Geophys. Res. Lett.*, 43, 4433–4440, doi:10.1002/2016GL068220.
- Rosier, S. H. R., G. H. Gudmundsson, and J. A. M. Green (2014), Insights into ice stream dynamics through modeling their response to tidal forcing, *Cryosphere*, 8(5), 1763–1775.
- Rosier, S. H. R., G. H. Gudmundsson, and J. A. M. Green (2015), Temporal variations in the flow of a large Antarctic ice stream controlled by tidally induced changes in the subglacial water system, *Cryosphere*, 9, 1649–1661.
- Ruina, A. (1983), Slip instability and state variable friction laws, *J. Geophys. Res.*, 88(B12), 10,359–10,370.
- Savage, H. M., and C. Marone (2007), Effects of shear velocity oscillations on stick-slip behavior in laboratory experiments, *J. Geophys. Res.*, 112, B02301, doi:10.1029/2005JB004238.
- Sayag, R., and M. G. Worster (2011), Elastic response of a grounded ice sheet coupled to a floating ice shelf, *Phys. Rev. E: Stat. Nonlinear Soft Matter Phys.*, 84(3), 036111.
- Sayag, R., and M. G. Worster (2013), Elastic dynamics and tidal migration of grounding lines modify subglacial lubrication and melting, *Geophys. Res. Lett.*, 40, 5877–5881, doi:10.1002/2013GL057942.
- Schoen, N., A. Zammit-Mangion, J. Rougier, T. Flament, F. Rémy, S. Luthcke, and J. Bamber (2015), Simultaneous solution for mass trends on the West Antarctic Ice Sheet, *Cryosphere*, 9(2), 805–819.
- Schoof, C. (2005), The effect of cavitation on glacier sliding, *Proc. R. Soc. A*, 461(2055), 609–627.
- Schulson, E. M., and A. L. Fortt (2012), Friction of ice on ice, *J. Geophys. Res.*, 117, B12204, doi:10.1029/2012JB009219.
- Segall, P., A. M. Rubin, A. M. Bradley, and J. R. Rice (2010), Dilatant strengthening as a mechanism for slow slip events, *J. Geophys. Res.*, 115, B12305, doi:10.1029/2010JB007449.
- Sergienko, O., T. Creyts, and R. Hindmarsh (2014), Similarity of organized patterns in driving and basal stresses of Antarctic and Greenland ice sheets beneath extensive areas of basal sliding, *Geophys. Res. Lett.*, 41, 3925–3932, doi:10.1002/2014GL059976.
- Sergienko, O. V., D. R. MacAyeal, and R. A. Bindschadler (2009), Stick–slip behavior of ice streams: Modeling investigations, *Ann. Glaciol.*, 50(52), 87–94.
- Shepherd, A., et al. (2012), A reconciled estimate of ice-sheet mass balance, *Science*, 338(6111), 1183–1189.

- Shibazaki, B., and Y. Iio (2003), On the physical mechanism of silent slip events along the deeper part of the seismogenic zone, *Geophys. Res. Lett.*, *30*(9), 1489, doi:10.1029/2003GL017047.
- Shibazaki, B., and T. Shimamoto (2007), Modelling of short-interval silent slip events in deeper subduction interfaces considering the frictional properties at the unstable-stable transition regime, *Geophys. J. Int.*, *171*(1), 191–205, doi:10.1111/j.1365-246x.2007.03434.x.
- Shimamoto, T. (1986), Transition between frictional slip and ductile flow for halite shear zones at room temperature, *Science*, *231*(4739), 711–714.
- Siegfried, M. R., H. A. Fricker, S. P. Carter, and S. Tulaczyk (2016), Episodic ice velocity fluctuations triggered by a subglacial flood in West Antarctica, *Geophys. Res. Lett.*, *43*, 2640–2648, doi:10.1002/2016GL067758.
- Smith, E., A. Smith, R. White, A. Brisbourne, and H. Pritchard (2015), Mapping the ice-bed interface characteristics of Rutford Ice Stream, West Antarctica, using microseismicity, *J. Geophys. Res. Earth Surf.*, *120*, 1881–1894, doi:10.1002/2015JF003587.
- Stearns, L. A., K. C. Jezek, and C. J. van der Veen (2005), Decadal-scale variations in ice flow along Whillans Ice Stream and its tributaries, West Antarctica, *J. Glaciol.*, *51*(172), 147–157.
- Suckale, J., J. D. Platt, T. Perol, and J. R. Rice (2014), Deformation-induced melting in the margins of the West Antarctic ice streams, *J. Geophys. Res. Earth Surf.*, *119*, 1004–1025, doi:10.1002/2013JF003008.
- Thomason, J. F., and N. R. Iverson (2008), A laboratory study of particle ploughing and pore-pressure feedback: A velocity-weakening mechanism for soft glacier beds, *J. Glaciol.*, *54*(184), 169–181, doi:10.3189/002214308784409008.
- Thompson, J., M. Simons, and V. C. Tsai (2014), Modeling the elastic transmission of tidal stresses to great distances inland in channelized ice streams, *Cryosphere*, *8*(6), 2007–2029.
- Tulaczyk, S., B. Kamb, R. P. Scherer, and H. F. Engelhardt (1998), Sedimentary processes at the base of a West Antarctic ice stream: Constraints from textural and compositional properties of subglacial debris, *J. Sediment. Res.*, *68*(3), 487–496.
- Tulaczyk, S., W. B. Kamb, and H. F. Engelhardt (2000), Basal mechanics of Ice Stream B, West Antarctica: 1. Till mechanics, *J. Geophys. Res.*, *105*(B1), 463–481, doi:10.1029/1999JB900329.
- Tulaczyk, S., et al. (2014), WISSARD at subglacial Lake Whillans, West Antarctica: Scientific operations and initial observations, *Ann. Glaciol.*, *55*(65), 51–58, doi:10.3189/2014AoG65A009.
- Vaughan, M. J., K. V. Wijk, D. J. Prior, and M. H. Bowman (2016), Monitoring the temperature-dependent elastic and anelastic properties in isotropic polycrystalline ice using resonant ultrasound spectroscopy, *Cryosphere*, *10*(6), 2821–2829.
- Viesca, R. C. (2016a), Self-similar slip instability on interfaces with rate- and state-dependent friction, *Proc. R. Soc. A*, *2192*, 20160254.
- Viesca, R. C. (2016b), Stable and unstable development of an interfacial sliding instability, *Phys. Rev. E*, *93*(6), 060202.
- Walker, R., B. Parizek, R. Alley, and S. Nowicki (2016), A viscoelastic model of ice stream flow with application to stick-slip motion, *Front. Earth Sci.*, *4*, 2.
- Walker, R. T., B. R. Parizek, R. B. Alley, S. Anandakrishnan, K. L. Riverman, and K. Christianson (2013), Ice-shelf tidal flexure and subglacial pressure variations, *Earth Planet. Sci. Lett.*, *361*, 422–428.
- Walter, J., I. Svetlizky, J. Fineberg, E. Brodsky, S. Tulaczyk, C. Barcheck, and S. Carter (2015), Rupture speed dependence on initial stress profiles: Insights from glacier and laboratory stick-slip, *Earth Planet. Sci. Lett.*, *411*, 112–120, doi:10.1016/j.epsl.2014.11.025.
- Walter, J. I., E. E. Brodsky, S. Tulaczyk, S. Y. Schwartz, and R. Petterson (2011), Transient slip events from near-field seismic and geodetic data on a glacier fault, Whillans Ice Plain, West Antarctica, *J. Geophys. Res.*, *116*, F01021, doi:10.1029/2010JF001754.
- Whillans, I., C. Bentley, and C. Van der Veen (2001), Ice Streams B and C, in *The West Antarctic Ice Sheet: Behavior and Environment*, edited by R. B. Alley and R. A. Bindschadler, pp. 257–281, AGU, Washington, D. C.
- Wiens, D. A., S. Anandakrishnan, J. P. Winberry, and M. A. King (2008), Simultaneous teleseismic and geodetic observations of the stick-slip motion of an Antarctic ice stream, *Nature*, *453*(7196), 770–774.
- Winberry, J. P., S. Anandakrishnan, R. B. Alley, R. A. Bindschadler, and M. A. King (2009), Basal mechanics of ice streams: Insights from the stick-slip motion of Whillans Ice Stream, West Antarctica, *J. Geophys. Res.*, *114*, F01016, doi:10.1029/2008JF001035.
- Winberry, J. P., S. Anandakrishnan, D. A. Wiens, R. B. Alley, and K. Christianson (2011), Dynamics of stick-slip motion, Whillans Ice Stream, Antarctica, *Earth Planet. Sci. Lett.*, *305*(3), 283–289.
- Winberry, J. P., S. Anandakrishnan, R. B. Alley, D. A. Wiens, and M. J. Pratt (2014a), Tidal pacing, skipped slips and the slowdown of Whillans Ice Stream, Antarctica, *J. Glaciol.*, *60*(222), 795–807, doi:10.3189/2014JoG14J038.
- Winberry, J., S. Anandakrishnan, and D. Wiens (2014b), Whillans stick-slip 2011, UNAVCO, doi:10.7283/T5SQ8XPC. GPS Data Set.
- Zoet, L., B. Carpenter, M. Scuderi, R. Alley, S. Anandakrishnan, C. Marone, and M. Jackson (2013), The effects of entrained debris on the basal sliding stability of a glacier, *J. Geophys. Res. Earth Surf.*, *118*, 656–666, doi:10.1002/jgrf.20052.
- Zoet, L. K., and N. R. Iverson (2015), Experimental determination of a double-valued drag relationship for glacier sliding, *J. Glaciol.*, *61*(225), 1–7.
- Zoet, L. K., and N. R. Iverson (2016), Rate-weakening drag during glacier sliding, *J. Geophys. Res. Earth Surf.*, *121*, 1206–1217, doi:10.1002/2016JF003909.
- Zoet, L. K., S. Anandakrishnan, R. B. Alley, A. A. Nyblade, and D. A. Wiens (2012), Motion of an Antarctic glacier by repeated tidally modulated earthquakes, *Nat. Geosci.*, *5*(9), 623–626, doi:10.1038/ngeo1555.